Fusion Engineering and Design 211 (2025) 114786

Contents lists available at ScienceDirect

Fusion Engineering and Design

journal homepage: www.elsevier.com/locate/fusengdes

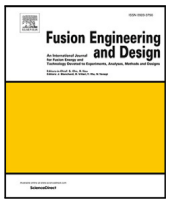

Impact of plasma diamagnetism and plasma currents on the superconducting field coils in Wendelstein 7-X

M. Endler *, K. Rißе, J. Geiger, K. Rahbarnia, M. Schneider, V. Bykov, M. Khokhlov, D. Zhang, W7-X Team[1]

Max–Planck-Institut für Plasmaphysik, Wendelsteinstraße 1, 17491 Greifswald, Germany

ARTICLE INFO

Keywords:
Superconducting magnets
Quench detection
Wendelstein 7-X
Magnetic diagnostics
Plasma energy

ABSTRACT

During operation of the Wendelstein 7-X stellarator, there were discharges with unusually fast plasma decay, which surprisingly triggered the quench detection system of the superconducting field coils, although no actual quench happened. We analyse the design of the field coils in conjunction with the particular technical set-up of the quench detection system and can model and quantitatively reproduce the observed behaviour. Several ways are proposed how the undesired effect could be mitigated. In addition, we discuss how the current and voltage signals of the field coils can be used in turn to derive diamagnetic energy and toroidal plasma current. The application is demonstrated, using signals from the existing machine control electronics, and reasonable agreement with the energy measurement of a diamagnetic loop is demonstrated.

1. Introduction

Wendelstein 7-X (W7-X) is a modular stellarator with superconducting field coils, average major radius of 5.5 m and average minor radius of 0.5 m [2,3]. It is located at the Max–Planck-Institut für Plasmaphysik in Greifswald. Its magnetic field is generated by 50 non-planar coils [4,5]. The magnetic configuration can be modified for experimental flexibility by a further set of 20 planar coils [5,6], which change the rotational transform and the vertical component of the magnetic field. The magnet system consists of five identical machine modules. Each module is composed of two half modules, which are flip-symmetric to each other. Each half module contains five different types of non-planar coil and two different types of planar coil, such that overall 10 coils of each of the 7 types are used in the toroidal arrangement of the 10 half modules (see [4, Figs. 1 and 2]). All 10 coils of one type are electrically connected in series, such that a set of 7 power supplies is used.

The winding packs of the coils and the bus system connecting the coils with each other and with the current leads consist of a cable-in-conduit conductor (CICC) with an aluminium jacket of square outer cross-section and circular hole in the centre, which contains strands of NbTi embedded in copper [7]. The coils can be operated at 4 K with currents of up to 18.2 kA, which will generate a magnetic field of up to 3 T on the plasma axis [4].

During operation, the circuit of each type of superconducting field coil is closed through its power supply. The coil current is therefore under permanent control. If a quench should occur somewhere in the CICC, ohmic heating will cause the normally conducting section to extend quickly along the conductor [8], heating it to ever higher temperatures and evaporating the liquid He coolant, such that finally thermal stress or even melting would destroy the coil. To avoid this, the quench must be quickly detected, and the coil current path is then changed from the power supply to a set of resistors to convert the entire magnetic energy into heat with a time constant of 5–7 s [9]. Such a fast ramp-down is initiated in all coil circuits simultaneously to avoid mechanical stress for which the coil system was not designed.

A quench is detected by measuring the voltages across sections of the windings and of the bus system connecting the coils. Under stationary currents along the superconductor, this voltage is 0, whereas a non-zero voltage will be measured in a section with final ohmic resistance due to a quench. If such a condition is detected for a sufficiently long validation time interval τ_{detect}, a fast ramp-down of the coil currents as described above is initiated. The time interval τ_{detect} is introduced to avoid triggering a fast ramp-down due to noise in the detection system. $\tau_{\mathrm{detect}} = 50\,\mathrm{ms}$ was originally set at W7-X. This is a short interval if compared with the toroidal field coils of other superconducting plasma confinement experiments like Tore Supra (1 s) [10], KSTAR (1–2 s) [11], EAST (1 s) [12], or ITER (1 s) [13] but comparable with the detection time in SST-1 (100 ms) [14]. The W7-X value of $\tau_{\mathrm{detect}} = 50\,\mathrm{ms}$ is the result of a thermo-hydraulic

* Corresponding author.
E-mail address: Endler@ipp.mpg.de (M. Endler).
[1] see [1] for the members of the W7-X Team.

https://doi.org/10.1016/j.fusengdes.2024.114786
Received 7 August 2024; Received in revised form 5 December 2024; Accepted 21 December 2024
Available online 17 January 2025

analysis of the particular CICC used (see Section 2.2).

Since W7-X has started operation in 2015 [15–17], there occurred two plasma events which triggered the quench detection (QD) system, without a quench having occurred anywhere in the superconductor. In both cases, the plasma had terminated more rapidly than in normal operation, i. e., the rate of change of the plasma diamagnetic energy and of the toroidal plasma current was larger than usually at the end of a discharge in W7-X. In both of the cases, a large amount of heavy impurities had been injected into the plasma core due to unfavourable operating conditions, such that the plasma energy was quickly radiated.

Although the W7-X device is designed to withstand several fast discharges of the coil currents, the mechanical stress in the coil system and in other components is higher than usually due to transient effects, high voltages occur between the coil windings and ground during the rapid change of coil current, and the carefully balanced flow of liquid He is perturbed by the sudden heating of the coil casings by eddy currents. Operation of the device is therefore interrupted for at least several hours after triggering a fast ramp-down of the coil currents. Hence, it is of interest to understand the conditions under which a change in plasma parameters will trigger the QD system. To this end, we shall explain in more detail the design of the W7-X superconducting field coils and of their QD system in Section 2. We shall show the observations of plasma diagnostics and the signals recorded by the QD system during a "fast" plasma decay in Section 3. In Section 4, we shall present a model of the voltages induced in the field coils, and compare the predictions of this model with the observed values. In Section 5, we shall discuss what modifications would help to avoid the undesired reaction of the QD system without blinding it for a real quench. As we shall see in these sections, the voltages induced in the field coils mainly reflect the changes of the plasma diamagnetic energy. We shall therefore discuss in Section 6, in what way measurements of the field coil currents and voltages can be used to complement the signals of magnetic pick-up coils (magnetic diagnostics) for the measurement of the plasma energy, before we shall discuss the results in Section 7 and conclude in Section 8.

2. The W7-X superconducting coils and quench detection system

2.1. Coils and design of the winding pack

The winding packs of the non-planar coils are formed by 108 windings of the CICC. These winding packs are supported by cast steel casings, to which they are connected by an interlayer of sand and resin. Two layers of superconductor with 18 turns are wound from one manufactured length of superconductor. The ends of this "double layer" (DL) are protruding from the winding pack and are connected by special joints either to the bus system or to the next DL. These joints also serve to feed the liquid He coolant into and out of the DLs. The entire winding pack is made from 6 DLs, which are electrically connected in series and arranged radially, such that DL1 encloses the smallest area and DL6 encloses the largest area (see Fig. 1). The design of these coils is described in more detail in [5,18].

The winding packs of the planar coils have a very similar design but consist of only 3 DLs with 12 windings each, making up a total of 36 windings.

In contrast, the winding layers of superconducting tokamak toroidal field coils are frequently arranged toroidally (in "pancakes" or "double pancakes") [10,13,14,19,20].

2.2. Quench detection system

If a section of the superconductor looses its superconductivity during operation, the current across the section with finite conductivity will cause a voltage drop, which can be measured. In W7-X, every section of superconductor is monitored by standardised quench detection units (QDUs) [21]. A QDU has 3 input lines, and the voltages between

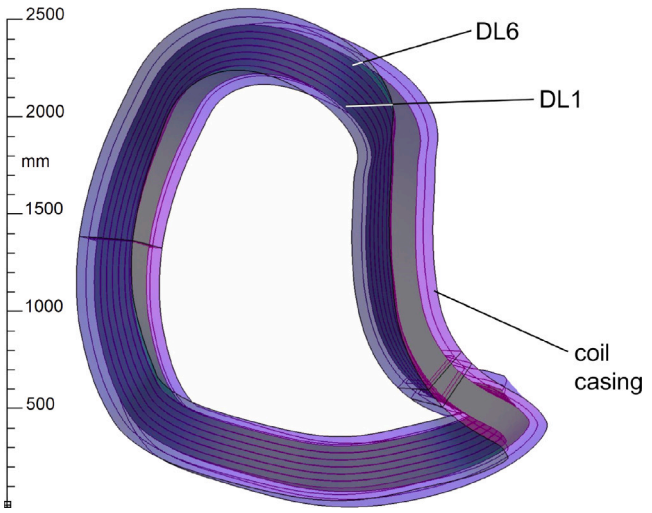

Fig. 1. View of a type 5 non-planar coil with its 6 double layers radially stacked and the coil casing (semi-transparent).

the common central line and the two other lines are compared (see simplified scheme in Fig. 2). Thus, the voltages across adjacent DLs or across adjacent sets of DLs can be compared. To this end, the input voltages are transmitted through a network of resistors to a differential amplifier (DA). The network of resistors basically forms two tunable bridges, such that the DA receives the difference of the two input voltages. The bridges are tunable in 128 steps to reduce either the first or the second input voltage. Effectively, this results in two input damping factors in each QDU, out of which one will be $= 1$ and the other will be ≤ 1. The output signal of the DA is further processed (see below) and at the same time recorded internally in a ring buffer with a sample rate of 100 kHz and a depth of 1 Msamples. One QDU can thus be used to compare two voltages, or to measure a single voltage, if one of the lateral input lines is connected to the central input line. The latter mode of operation is used to measure the voltage across a section of the superconducting bus connecting the coils of one circuit, the first mode is used to compare the voltages across DLs in a coil.

The output signal of the DA passes through an integrator (RC circuit with adjustable resistor) to a comparator. The RC circuit realises the delay τ_{detect} mentioned in Section 1. The delay is, in fact, not a fixed time. Rather, the time constant of the RC circuit is identified with τ_{detect}. If the integrated signal exceeds an adjustable threshold voltage, the QDU will change its logical output signal, indicating to a QD subsystem that a quench condition was detected [22,23]. The signals of the different QD subsystems are then combined by a QD interface, which will initiate a fast ramp-down of all coil currents if any QDU outputs such a trigger signal. In addition, the ring buffers of all QDUs will be written to an external storage system, such that ~ 5 s before and ~ 5 s after the trigger event are recorded of all QD signals for later analysis.

Within each QDU, the comparator, decision logic and output to the QD subsystem are redundant. In addition, a broken wire between coil and QDU can be detected. In a non-planar coil, there are three QDUs forming the "original system" which compare the voltages across DL1 and DL2, DL3 and DL4, and DL5 and DL6, respectively, and a fourth QDU, comparing the voltage across DLs 1 and 2 with the voltage across DLs 3–6 ("backup system"), introducing a further layer of redundancy.

As mentioned in Section 1, as soon as a quench occurs, the normally conducting section will start spreading along the conductor, while the temperature is increasing [8]. At the same time, the voltage drop across the affected section of conductor starts increasing. In order to avoid damage to the quenching coil due to thermal stress, the hot spot temperature in the coil should be limited to 130 K. Thermo-hydraulic

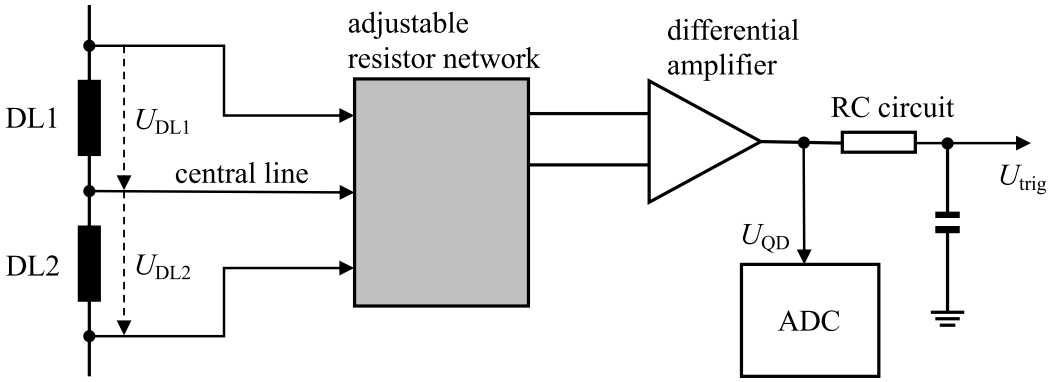

Fig. 2. Simplified scheme of a quench detection unit (QDU): The output of the resistor network and the differential amplifier is the QD voltage $U_{QD} = d_2 U_{DL2} - d_1 U_{DL1}$ (where d_1, d_2 are adjustable damping factors, see Eq. (5)), which is written into a ring buffer but only archived upon request (e. g., automatically in case the QD system is triggered). An RC circuit serves as integrator to generate a trigger voltage U_{trig} which is directly compared with an adjustable trigger threshold.

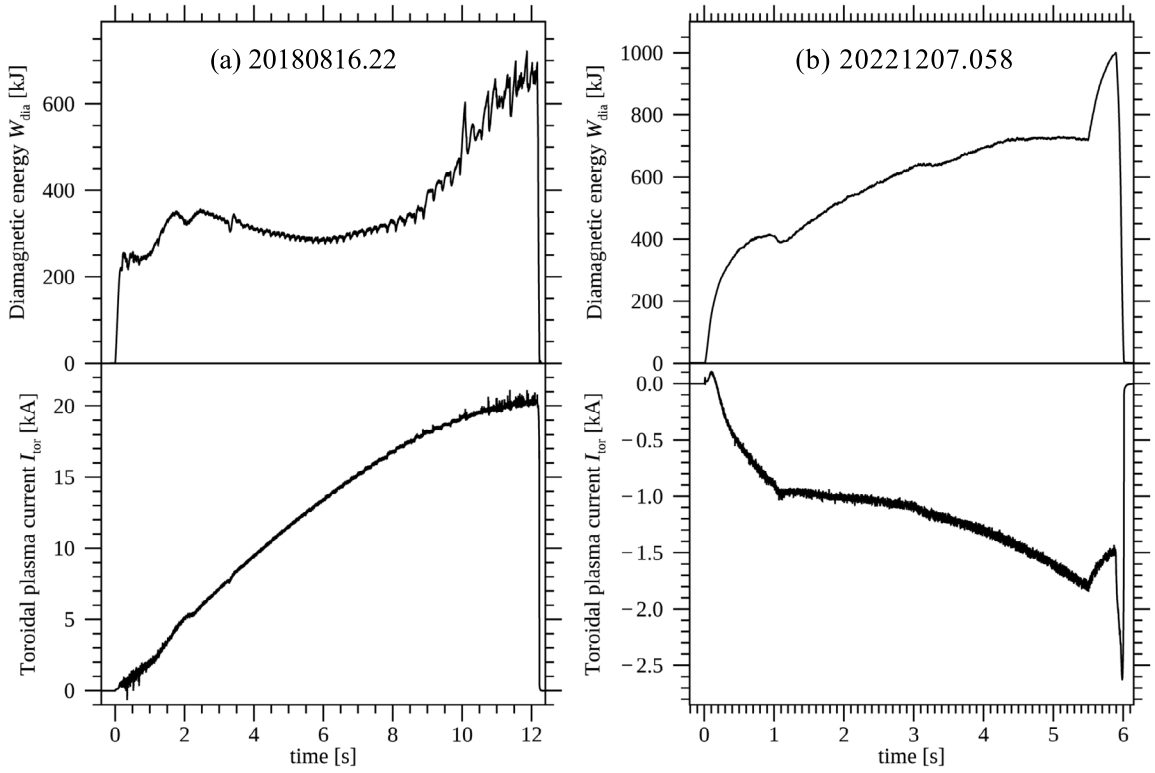

Fig. 3. Full time windows of W_{dia} and I_{tor} in the two W7-X discharges at the end of which, due to an extraordinarily fast plasma decay, the QD system triggered a fast ramp-down of the coil currents.

analysis of such an event for the particular CICC and the conditions at 2.5 T operation in W7-X together with the time needed for a fast ramp-down of the coil currents shows that then the ramp-down must start ~950 ms after the quench occurs [24]. It will take ~250 ms before the voltage exceeds the threshold value of the QDU, plus the delay $\sim \tau_{detect}$ due to the integration, plus ~350 ms before the current breakers have switched the coil currents to the resistors, and the coil currents start to decrease. From simulations of temperature and ohmic resistance in a quenching coil in the thermo-hydraulic model, tolerable combinations of threshold voltage and validation time can then be derived [24]. Allowing for some safety margin, the initial settings in the QDUs were threshold voltages of 150 mV for the "original system" (DLs 1–2, 3–4 and 5–6) and 300 mV for the "backup system" (DLs (1+2)–(3+4+5+6)), and a validation time (RC of the integrator) of ~50 ms.

3. Observations during "fast" plasma decay

In Fig. 3, we show the diamagnetic energy W_{dia} and the toroidal plasma current I_{tor} during the two discharges ending with extraordinarily fast decay of the plasma, as measured by a diamagnetic loop and a Rogowski coil (for an overview of the W7-X magnetic diagnostics, see [25], and for more details on the W_{dia} measurements, see [26]). In Fig. 4, the phases of the plasma decay are enlarged, and the radiation measured by bolometer cameras [27] is shown in Fig. 5. In both cases, the total loss of plasma energy according to the diamagnetic signal matches well the radiated energy in the same interval (see Table 1). In contrast, the power load to the targets did not significantly increase, as one might expect if the end of the discharge would be due to an MHD instability. Indeed, as the 2018 discharge had a toroidal plasma current of almost 20 kA due to electron cyclotron current drive (ECCD) in the co-direction, minor crashes in plasma energy and oscillations

Table 1
Radiative losses (integrated radiated power P_{rad}) in the intervals of fast plasma decay (as defined by $[t_1, t_2]$, compare Figs. 4 and 5) in discharges 20180816.022 and 20221207.058. The first discharge was heated with a heating power P_{heat} of 3.5 MW ECRH, the second discharge was heated with 3 MW ECRH and 3.6 MW NBI, of which ~70% are absorbed during the main phase of the discharge. It is not known which fraction of the heating power is still absorbed during the plasma decay. If we assume that still 30% of the heating power are absorbed during the decay phase, most of the plasma energy is lost due to radiation.

Discharge no.	20180816.022	20221207.058
ΔW_{dia}	0.7 MJ	1.0 MJ
t_1	12.16 s	5.89 s
t_2	12.24 s	6.02 s
$\int_{t_1}^{t_2} P_{rad}\,dt$	0.7 … 0.8 MJ	~1.2 MJ
$\int_{t_1}^{t_2} P_{heat}\,dt$	0.3 MJ	0.7 MJ

in plasma current occurred prior to the final decay (see Fig. 3), due to current-driven instability [28,29]. It had therefore for some time been conjectured that this instability also caused the final fast decay. However, due to the analyses of the radiation levels, which had become available later, we conclude that in both cases the fast loss of plasma energy was indeed due to strong impurity radiation by tungsten, from the multi-purpose manipulator [30] in 20180816.022 due to a plunge depth which was poorly adapted to the magnetic configuration modified by the high plasma current [31], and from a tungsten-coated heat shield tile in 20221207.058, which was receiving a high load of microwave radiation due to an unfavourable setting of an ECRH (Electron Cyclotron Resonance Heating) launcher. Tungsten as a strong radiator during the plasma decay phases is in both cases confirmed by the HEXOS VUV/XUV spectrometer [32]. We note that both events resulted in a similar maximum decay rate of the diamagnetic energy, as indicated in Fig. 4. The net toroidal plasma current at the moment of the event was almost 20 kA in 20180816.022 but only 1.5 kA in 20221207.058 without ECCD. We further note that the net plasma current in both cases first reacts only weakly due to the long L/R time for the toroidal current in W7-X of several seconds. As soon as there is, towards the end of the decay phase of the diamagnetic energy, no longer sufficient plasma left to carry the current, the plasma current rapidly decays to zero within a few milliseconds.

We shall use 20221207.058 to investigate and model the impact of the fast plasma decay on the field coils. In Fig. 6 we display the voltages recorded in the four QDUs monitoring one particular non-planar coil of type 5, AAB16. The QDU of the "backup system", comparing the voltage across DL1+2 with the voltage across DL3+4+5+6, was the one triggering the fast ramp-down of the coil currents. The QD signals of the other non-planar field coils are similar. Their temporal evolution is very similar for corresponding QDUs of different coils. Likewise, the amplitudes in corresponding QDUs of different coils are very similar for coils of the same type in different half modules and differ more between the different coil types, but many of them also exceed the trigger thresholds.

4. Modelling of the voltages induced in the field coils

In this section, we shall develop our model to describe the interaction between plasma and field coils and to understand the origin of the voltages observed in the QD system. In a stepwise approach, we shall first develop a basic understanding of the electromagnetic interaction between plasma, plasma vessel and field coils in Section 4.1. We shall then describe mathematically the interaction between plasma and the superconducting coil circuits and discuss the calculated voltages in the QD system for two examples in Section 4.2. We shall then consider the influence of plasma vessel and coil casing, which are also inductively coupled to the plasma and to the superconducting windings, in a simplified numerical model in Section 4.3. Finally, we shall compose the different elements into the complete model and compare its results with the measured signals during the fast plasma decay at the end of discharge 20221207.058 in Section 4.4.

4.1. Qualitative considerations

4.1.1. Plasma diamagnetism

The gyration of the plasma particles reduces the externally applied magnetic field in the volume filled by the plasma. This effect increases with increasing plasma density and temperature. (Since the effect originates in the movement of the charged particles perpendicular to the magnetic field, only the temperature component perpendicular to the magnetic field counts, which must be taken into account if the temperature is not isotropic [33,34].)

The magnetic flux through a closed loop around the plasma column is determined, in addition to the externally applied magnetic field, by the diamagnetic effect as well as by plasma currents parallel to the magnetic field [35,36]. We shall first consider the diamagnetic effect and discuss the effect of parallel currents in Section 4.1.2. In the approximation of large aspect ratio and low β, the change of the magnetic flux Φ_{dia} for plasma energy W, magnetic vacuum field on the plasma axis B_0 and major radius R will then be

$$\Phi_{dia} = -\frac{\mu_0 W}{3\pi R B_0}. \quad (1)$$

The negative sign indicates the reduction of the magnetic field relative to the vacuum case. Use is made of the plasma diamagnetism by measuring the voltage induced in a *diamagnetic loop*, a pick-up coil with poloidal winding around the plasma column. Three such diamagnetic loops are installed in W7-X [25,26], and use is made mostly of that located in a plane with triangular plasma cross-section ("triangular plane", see Fig. 7), which will also be referred to as "main diamagnetic loop". By integrating the induced voltage in a diamagnetic loop from the start of a plasma discharge, a measure of the plasma energy is available at any time of the discharge. Since changes in the toroidal magnetic field due to changes in the field coil currents will also induce a voltage in a diamagnetic loop, such changes must be compensated by *compensation coils* which enclose an area in the same plane as the diamagnetic loop without enclosing the plasma column itself.

In a toroidal plasma with helical magnetic field, and in particular in a stellarator configuration, which is no longer toroidally symmetric and may have toroidal variations of the magnetic field and the major radius of the plasma axis, the relation between Φ_{dia} and the kinetic plasma energy W_{kin} is still predominantly linear, but the factor of proportionality may differ from Eq. (1) and depends on the exact shape and location of the poloidal loop around the plasma column. This factor of proportionality can be determined by calculating the magnetic flux which a plasma equilibrium with certain radial profiles of plasma pressure and parallel current density generates in the pick-up coil to be considered. We use the DIAGNO code [37] for this purpose. We note that the factor of proportionality of a fixed flux loop may also depend on the magnetic configuration and on the shape of the pressure profile. We therefore refer to the energy calculated from Φ_{dia} as W_{dia} to distinguish it from W_{kin}.

For the *compensated* diamagnetic signal of the main diamagnetic loop in W7-X, W_{dia} of Eq. (1) happens to agree with W_{kin} within 1–2% for the magnetic "standard" configuration (this is the configuration with equal currents in all non-planar coils and zero currents in the planar coils — for an overview on the W7-X magnetic configuration space, see [38]), if the major radius of the plasma axis in the plane of this diamagnetic loop is used for R, and the magnetic field on the axis in this plane for B_0, i. e., $R = 5.25\,m$ and $B_0 \approx 2.4\,T$ in discharge 20221207.058. For $W_{dia} = 1\,MJ$ we then obtain $\Phi_{dia} \approx -10\,mVs$. In a long cylinder with 0.5 m radius, such a change in the magnetic flux would be generated by an azimuthal current density of ~10 kA/m, which corresponds to a total poloidal current of ~350 kA on the plasma surface of W7-X. The single-loop voltage induced by the plasma energy

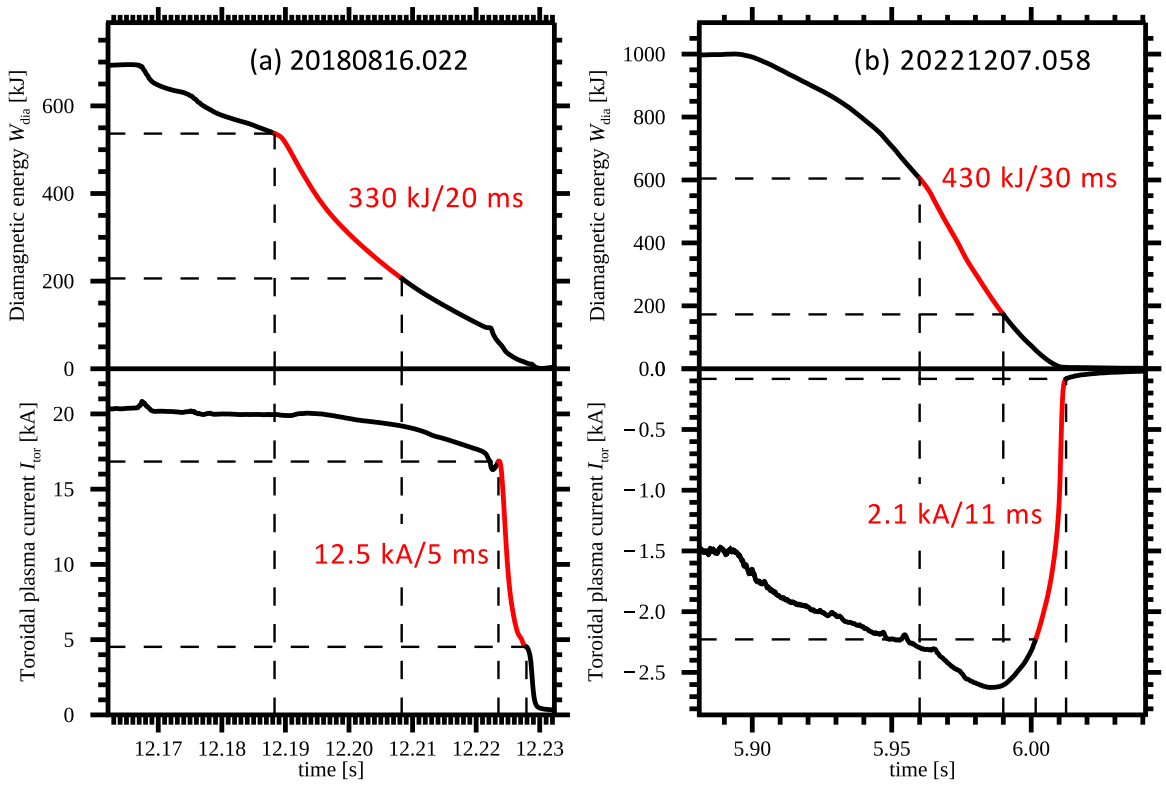

Fig. 4. Decays of W_{dia} and I_{tor} at the end of the two W7-X discharges 20180816.022 and 20221207.058. The strongest decay rates are indicated in red. The changes in coil current in response to the decays are shown in Fig. 8. The value of 430 kJ/30 ms for the decay of W_{dia} in discharge 20221207.058 will be used as a reference in our discussion of the effect on the field coils in Section 4.

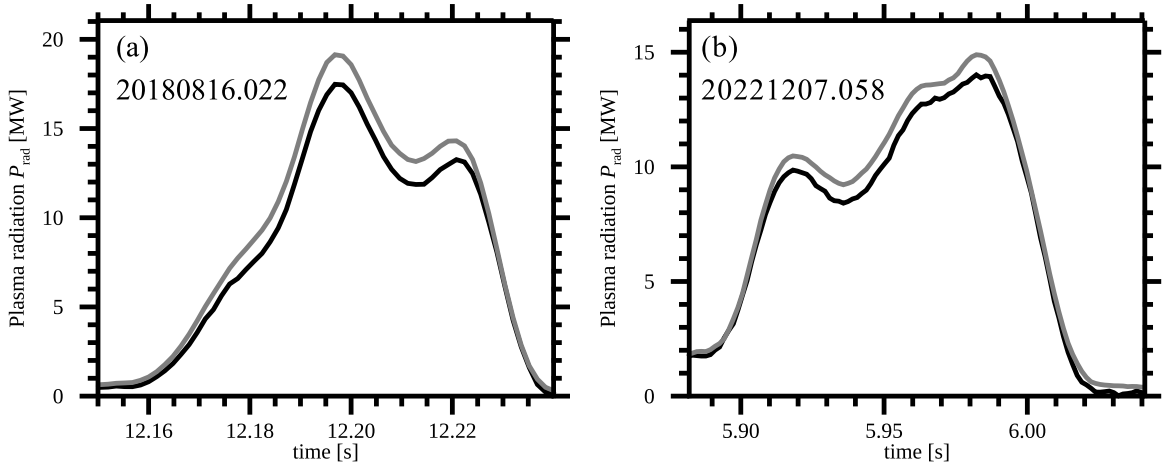

Fig. 5. Total plasma radiation P_{rad} as calculated from bolometric measurements with the horizontal (black) and vertical (grey) bolometer cameras [27] during the intervals of plasma decay in discharges 20180816.022 and 20221207.058. The radiated power integrated over the intervals of plasma decay corresponds rather well to the diamagnetic energy before the start of the decay (see Table 1).

decay of 430 kJ/30 ms indicated in Fig. 4 for the end of discharge 20221207.058 would then be ~150 mV.

We note that every non-planar or planar W7-X field coil also satisfies the geometric conditions of a diamagnetic loop. However, while a pick-up coil is terminated with a comparatively high ohmic impedance, such that the induced current will not significantly alter the magnetic flux through the winding, the opposite is true for the field coils: If the coil current changes by ΔI in response to a change in Φ_{dia} (see Fig. 8), this change will itself modify the flux through the coil. If the coil winding consists of several radially stacked DLs enclosing different areas, the changes in magnetic flux through the different DLs due to ΔI is no longer equal (see the CAD view of a type 5 non-planar coil in Fig. 1).

4.1.2. Plasma currents

In addition to the diamagnetic effect, electric currents in the plasma may generate magnetic flux through external coils, which is used by further magnetic diagnostics [25]. The parallel current density is usually averaged over flux surfaces, yielding a radial profile of net current density, the bootstrap current. The remaining current densities with poloidal variation on a flux surface are usually called Pfirsch–Schlüter currents. Additional toroidal net currents may be driven by toroidally non-symmetric plasma heating. For W7-X, the minimisation both of the bootstrap current and of the Pfirsch–Schlüter currents was one of the optimisation criteria [39]. Nevertheless, changes in the net toroidal current or in the distribution of current densities will in general

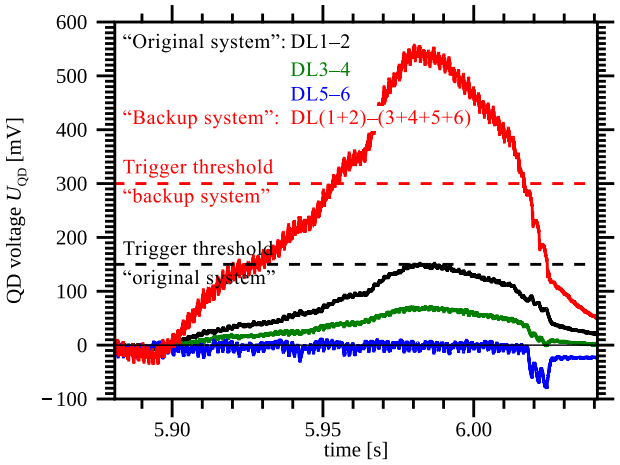

Fig. 6. Voltages recorded by the 4 quench detection units (QDUs) monitoring coil AAB16 during the fast plasma decay at the end of discharge 20221207.058. The AAB16 "backup system" QDU triggered the fast ramp-down of the coil currents in this discharge.

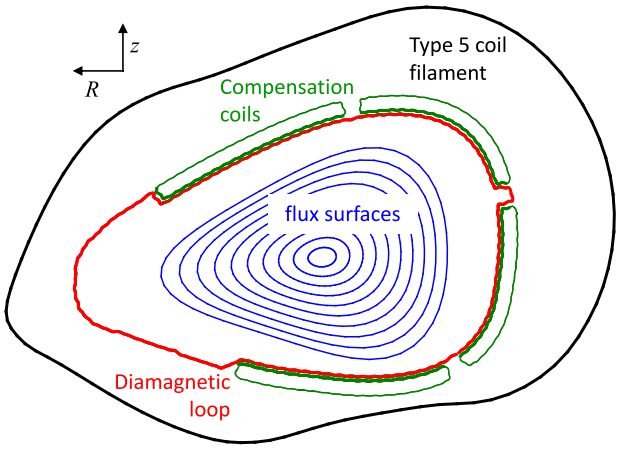

Fig. 7. Diamagnetic loop and 4 compensation coils in the plane with triangular plasma shape. A cross section through the magnetic flux surfaces and a projection of the filamentary representation of the winding of the type 5 non-planar field coil are also depicted. R is the major radial coordinate of the torus, z the vertical coordinate.

induce changes in the magnetic flux through coils outside the plasma.

The diamagnetic loop in the triangular plane (see Section 4.1.1) has been specifically designed to minimise the influence of plasma currents. The coupling of the field coils to toroidal plasma currents is stronger. In Table 2, we compare the flux change in the 7 types of field coil and in the main diamagnetic loop (including compensation) for a change of the plasma energy W_{kin} of 1 MJ and of the toroidal net current of 10 kA. The DIAGNO code [37] was used to obtain these values, which uses the current densities calculated in an equilibrium code to compute the magnetic flux through any desired coil geometry. DIAGNO had been used before to assess the sensitivity of the W7-X magnetic diagnostics to different current distributions [40], but the field coils had not yet been considered. The values in Table 2 are based on a parameterisation of results of DIAGNO for 106 equilibria in the W7-X "standard" magnetic configuration with different plasma energies, toroidal currents and two types of radial plasma pressure and toroidal current density profiles.

4.1.3. Dissipative components: plasma vessel and coil casing

Between the plasma with its changing diamagnetism and current distribution and the superconducting windings of the field coils, the plasma vessel and the coil casings are located. Before changes of the magnetic flux through the windings occur, shielding currents are induced in these steel structures, which will then decay due to ohmic dissipation on the characteristic L/R time scales, which are for the plasma vessel 17 ms for poloidal currents and 25–50 ms for toroidal currents [41] and ~25 ms for the non-planar coil casings at a temperature of 4 K. Faster changes in the magnetic flux originating inside the plasma vessel will be damped and delayed for the superconducting windings, as will be demonstrated by the simulation with simplified geometry in Section 4.3.

4.2. Modelling the linear response of the coil system

4.2.1. Changes of coil currents

For the mathematical description to be developed in this section, we shall neglect the plasma vessel and the coil casings. We shall consider them in the numerical model of Section 4.3, where we find that the effect of these dissipative elements does not alter the quantitative results dramatically, and where we introduce a simple numerical procedure to mimic their effect.

While the change in the coil current ΔI is the same in every DL, since the DLs are electrically connected in series, the change in magnetic flux through one DL by ΔI in any other DL varies due to their radial stacking. This is of course exactly what is described by the self and cross inductances of the DLs. Hence, a well established formalism exists to describe these electric circuits, which will at the same time take account of the 3-dimensional coil shapes, of the coil positions, and of the interactions between the 7 coil circuits, once the self and cross inductances of all DLs are calculated from their geometries.

The coil circuits can then be described by the system of linear equations (see, e. g., [13])

$$0 = U_{\mathrm{ext}\,j} - R_j I_j - \sum_{k=1}^{7} L_{jk} \frac{\mathrm{d}I_k}{\mathrm{d}t} - \frac{\mathrm{d}\Phi_{\mathrm{plasma}\,j}}{\mathrm{d}t} \quad (j = 1, \ldots, 7). \tag{2}$$

The ohmic resistance in the circuits R_j is dominated by the normal conducting aluminium current leads between the power supplies and the torus, and it is between 30 μΩ and 60 μΩ for the different circuits [42], resulting in a voltage drop of ~0.5–1 V at a typical coil current of 15 kA. The L_{jk} are the self and cross inductances of the entire coil circuits. The $\mathrm{d}\Phi_{\mathrm{plasma}\,j}/\mathrm{d}t$ can be subdivided into a contribution from plasma diamagnetism and a contribution from the plasma current density parallel to the magnetic field:

$$\frac{\mathrm{d}\Phi_{\mathrm{plasma}\,j}}{\mathrm{d}t} = \frac{\mathrm{d}\Phi_{\mathrm{dia}\,j}}{\mathrm{d}t} + \frac{\mathrm{d}\Phi_{\mathrm{pc}\,j}}{\mathrm{d}t} \tag{3}$$

$\mathrm{d}\Phi_{\mathrm{dia}\,j}/\mathrm{d}t$ and $\mathrm{d}\Phi_{\mathrm{pc}\,j}/\mathrm{d}t$ may both vary for the different coil types, and within one coil, there are small differences between the DLs (see Table 2).

4.2.2. Voltages across double layers

Eqs. (2) can be broken down to the contributions of individual DLs. The voltage across DL J in a coil of type j is

$$U_{Jj} = \underbrace{-\sum_{k=1}^{7} L_{\mathrm{DL}\,Jjk} \frac{\mathrm{d}I_k}{\mathrm{d}t}}_{\text{term 1}} \underbrace{- \frac{\mathrm{d}\Phi_{\mathrm{plasma}\,Jj}}{\mathrm{d}t}}_{\text{term 2}}. \tag{4}$$

Here, $L_{\mathrm{DL}\,Jjk}$ is the cross inductance of the single DL J in coil type j with all coils of type k. $L_{\mathrm{DL}\,Jjj}$ then includes the self inductance of DL J itself, the cross inductances of DL J with the other DLs of the same coil, and the cross inductances of DL J with the other 9 coils of the same type, which all carry the same current I_j. Correspondingly, $L_{\mathrm{DL}\,Jjk}$ for $j \neq k$ includes the cross inductances of DL J in one coil of type j with all 10 coils of type k. The $\mathrm{d}\Phi_{\mathrm{plasma}\,Jj}/\mathrm{d}t$ are the changes of the magnetic flux through one DL J of coil type j due to changes of the diamagnetic energy and of plasma currents. "Term 1" and "term 2" will be referred to below.

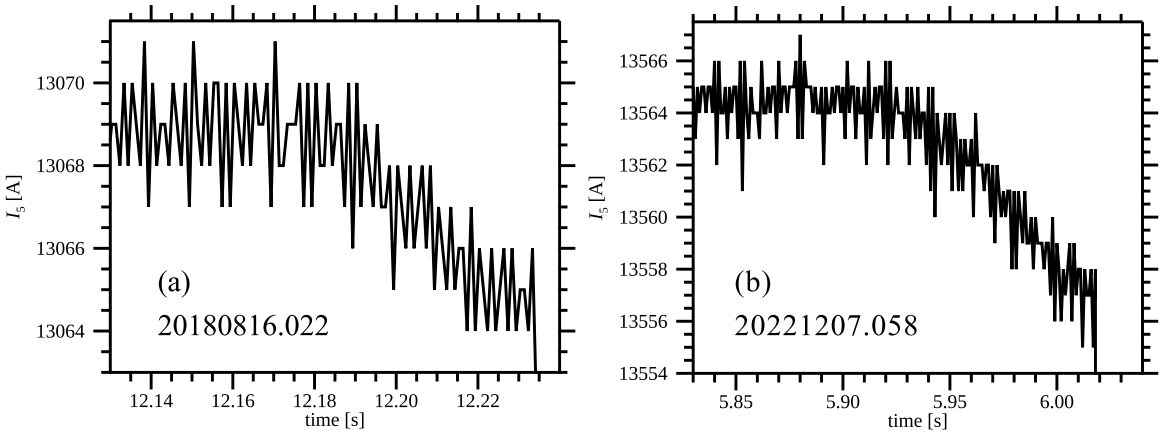

Fig. 8. Change in the coil currents of the non-planar coils of type 5 at the end of discharges 20180816.022 and 20221207.058, in response to the fast decay of W_{dia} (compare Fig. 4).

Table 2
Flux changes in mVs through the windings of the main diamagnetic loop (with compensation, leftmost column) and of the field coils. For comparison, the results for typical values of the plasma energy (upper half of the table) and of the toroidal plasma current (lower half of the table) in W7-X are given. The values are based on DIAGNO results for equilibria with different plasma energy and toroidal current in "standard" magnetic configuration (same current in all non-planar coil types, zero current in all other field coils). For the DIAGNO analysis, the coils are approximated by filaments in the centre of the winding or of the respective double layer. To be better comparable, all values are for single loops without taking into account the number of windings.

$\Delta W_{kin} = 1$ MJ	(All values in mVs)							
Diam. loop triang.		Field coil type						
plane (compensated)	Double layer	1	2	3	4	5	A	B
−10.6	all	−10.1	−9.7	−9.2	−9.1	−9.4	−11.4	−8.3
	innermost	−9.9	−9.4	−8.9	−8.9	−9.5	−11.3	−8.3
	outermost	−10.3	−10.0	−9.5	−9.2	−9.3	−11.4	−8.3
$\Delta I_{tor} = 10$ kA								
Diam. loop triang.		Field coil type						
plane (compensated)	Double layer	1	2	3	4	5	A	B
−0.12	all	+1.09	+1.20	+1.34	+1.33	+1.29	−0.30	+1.30
	innermost	+1.04	+1.16	+1.29	+1.26	+1.18	−0.28	+1.24
	outermost	+1.13	+1.24	+1.39	+1.39	+1.40	−0.32	+1.35

Table 3
Cross inductances of double layers 1 and 2 of coil type 5 with all coil types in mH, as used in Eqs. (4) and (6). The values serve as examples, demonstrating how little the values for double layers 1 and 2 differ. The differences of these values determine the differences in the voltages induced in double layers 1 and 2 if the coil currents change. The resulting voltages for several scenarios causing coil current changes are listed in Table 4.

All values in mH	L_{DLJ51}	L_{DLJ52}	L_{DLJ53}	L_{DLJ54}	L_{DLJ55}	L_{DLJ56}	L_{DLJ57}
$J = 1$	0.417	0.552	0.982	2.465	9.407	0.316	1.348
$J = 2$	0.443	0.586	1.038	2.585	10.276	0.336	1.449
Difference	6.2%	6.2%	5.7%	4.9%	9.3%	6.3%	7.5%

For each non-planar coil of type j ($j = 1, \ldots, 5$), four QDUs measure the voltages

$$\begin{aligned} U_{QD\,1-2,\,j} &= d_2 U_{2j} - d_1 U_{1j} \\ U_{QD\,3-4,\,j} &= d_4 U_{4j} - d_3 U_{3j} \\ U_{QD\,5-6,\,j} &= d_6 U_{6j} - d_5 U_{5j} \\ U_{QD\,bu,\,j} &= d_{bu2} \sum_{J=3}^{6} U_{Jj} - d_{bu1}(U_{1j} + U_{2j}). \end{aligned} \tag{5}$$

For each planar coil of type j ($j = 6, 7$ or A, B), three QDUs measure the voltages

$$\begin{aligned} U_{QD\,1-2,\,j} &= d_2 U_{2j} - d_1 U_{1j} \\ U_{QD\,2-3,\,j} &= d_3 U_{3j} - d_4 U_{2j} \\ U_{QD\,bu,\,j} &= d_{bu2}(U_{2j} + U_{3j}) - d_{bu1} U_{1j}. \end{aligned}$$

The factors d are the damping factors resulting from the tunable bridges at the input of the QDUs (see Section 2.2).

Hence,

$$\begin{aligned} U_{QD\,1-2,\,j} = &\sum_{k=1}^{7} (d_1 L_{DL\,1jk} - d_2 L_{DL\,2jk}) \frac{dI_k}{dt} \\ &+ d_1 \frac{d\Phi_{plasma\,1j}}{dt} - d_2 \frac{d\Phi_{plasma\,2j}}{dt}, \end{aligned} \tag{6}$$

etc. for the other QD voltages.

We note that the differences like $(L_{DL\,1jk} - L_{DL\,2jk})$ (and other pairings of DLs) are small in comparison with the values $L_{DL\,Jjk}$ themselves (see Table 3 for examples). The same is true for the $(d\Phi_{plasma\,1j}/dt - d\Phi_{plasma\,2j}/dt)$. The damping factors d are close to 1 for the "original system". But for fast changes of Φ_{plasma}, also the differences U_{jJ} of Eq. (4) will be small in comparison with the two addends. In a comparison between calculated and measured QD voltages it is therefore important to use precise values for the calculated self and cross inductances, and also the damping factors and the QD voltage within the QDU must be accurately known.

Table 4
Voltages U_{J5} across the 6 double layers of a type 5 non-planar coil for three scenarios, (1) coil excitation with 30 A/s, (2) change of the plasma energy with a rate of (−14 MJ/s) (like in discharge 20221207.058), generating a single-loop voltage of $d\Phi_{dia}/dt \sim 150$ mV in a poloidal winding with compensation coil (or ∼134 mV without compensation coil), and (3) change of a toroidal plasma current with a rate of (−400 kA/s) (like in discharge 20180816.022). The flux changes in the latter two scenarios have been calculated by parameterisation of DIAGNO code [37] results for "standard" magnetic configuration. Triangular radial plasma pressure and toroidal plasma current density profiles were assumed in the underlying equilibria. In addition, the voltage differences U_{QD} measured by the QDUs are tabulated, once without the damping factors d in Eq. (5) and once with the specific damping factors of coil AAB16 (listed in the last line of the table). In scenarios (2) and (3), "term 1" and "term 2" refer to Eq. (4), and "total" is the sum of the two terms. In the coil excitation scenario, "term 2" is zero.

All values	Coil excitation	$d\Phi_{dia}/dt \approx +150$ mV			$dI_{tor}/dt = -400$ kA/s		
in mV	with 30 A/s	total	term 1	term 2	total	term 1	term 2
U_{15}	−415	−294	+2 107	−2 400	+27	−824	+851
U_{25}	−448	−113	+2 276	−2 389	−8	−889	+881
U_{35}	−472	+20	+2 398	−2 378	−25	−937	+912
U_{45}	−486	+109	+2 476	−2 368	−25	−969	+944
U_{55}	−492	+148	+2 506	−2 358	−6	−982	+977
U_{65}	−485	+131	+2 480	−2 349	+35	−975	+1 010
without damping factors d in Eq. (5):							
$U_{QD\,1-2,5}$	−33	+181	+169	+12	−35	−65	+30
$U_{QD\,3-4,5}$	−15	+88	+78	+10	0	−31	+32
$U_{QD\,5-6,5}$	+6	−17	−26	+9	+41	+7	+34
$U_{QD\,bu,5}$	−1 073	+815	+5 479	−4 664	−39	−2 150	+2 110
with damping factors d of AAB16:							
$U_{QD\,1-2,AAB16}$	+30	+196	−150	+346	−34	+59	−93
$U_{QD\,3-4,AAB16}$	+5	+84	−21	+105	+1	+7	−6
$U_{QD\,5-6,AAB16}$	−28	−7	+150	−156	+41	−61	+102
$U_{QD\,bu,AAB16}$	−47	+599	+253	+346	−29	−103	+74
($d_1 = 1$, $d_2 = 0.86$, $d_3 = 1$, $d_4 = 0.96$, $d_5 = 0.93$, $d_6 = 1$, $d_{bu1} = 1$, $d_{bu2} = 0.47$)							

In the following two subsections we shall as two examples consider the excitation of the coil system and the reaction to the fast plasma decay in discharge 20221207.058 for a coil of type 5.

4.2.3. Application 1: Excitation of coil currents

When the superconducting coils are excited from zero current to achieve some desired magnetic configuration, the power supplies are programmed to generate linear current ramps to the set coil currents. As an example, we shall consider the "standard" magnetic configuration, which requires equal currents I in all types of non-planar coil and 0 current in the planar coils. For a magnetic field of 2.5 T on the plasma axis, the required non-planar coil currents are ∼13 kA. According to Eq. (2), for this magnetic configuration,

$$U_{ext\,j} - R_j I = \frac{dI}{dt} \sum_{k=1}^{5} L_{jk} \quad (j = 1, \ldots, 5).$$

The self inductances of the non-planar coil circuits vary between 0.52 H and 0.65 H, but the sums $\sum_{k=1}^{5} L_{jk}$ vary less, between 0.93 H and 0.98 H. The maximum voltage of the power supplies is 30 V, which allows for current ramps of ∼30 A/s, requiring ∼7 min for the full excitation of the coils in this configuration.

The resulting voltages across the DLs of a type 5 non-planar coil according to Eq. (4) are tabulated in Table 4 and represented graphically in Fig. 9. The total voltage difference along the winding of a single coil is 1/10 of the total applied voltage ($U_{ext\,5} - R_5 I$), but it is not entirely equally distributed to the different DLs (red curve versus black line in Fig. 9). Rather, the voltages across the DLs deviate by up to 11% from 1/6 of the total voltage across the entire winding.

In addition to the voltages across the DLs, the voltage differences measured by the 4 QDUs monitoring such a coil are also tabulated in Table 4, first without taking into account the input damping factors d of the QDUs (see Eq. (5)), then with the d values of coil AAB16. The purpose of the damping factors becomes obvious, to reduce the output voltage of the comparators of the QDUs, such that the QD system is not triggered during a regular excitation or de-excitation of the coils (in particular by the "backup" QDUs).

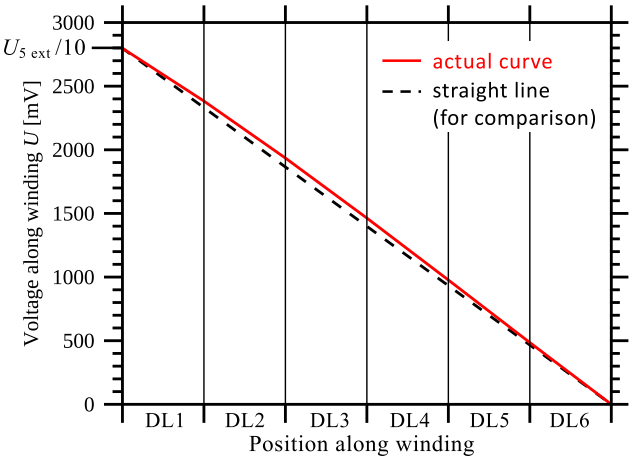

Fig. 9. Voltage along the winding of a type 5 coil during excitation with 30 A/s. The actual curve (red) deviates slightly from a straight line, which would be expected if the voltages across all DLs were equal.

4.2.4. Application 2: Fast decay of plasma energy or toroidal plasma current

Our second example considers a change in the coil currents induced by changes in the plasma energy or in the toroidal plasma current. We use the case of $dW_{dia}/dt = -420$ kJ/30 ms in discharge 20221207.058, resulting in a single-loop voltage of ∼150 mV (see Section 4.1.1), and we assume as a second separate scenario the contribution of $dI_{tor}/dt = -12$ kA/30 ms. Although a much faster decay of the toroidal plasma current was observed, e. g., in discharge 20180816.022, the toroidal eddy current induced in the plasma vessel will shield such a fast decay from the field coils. Apart from this, we do not take into account the damping effects of plasma vessel and coil casing here, which will be treated in Section 4.3. Considering Eq. (2), the power supplies do not react to the induced changes of the coil currents on the time scale of 20–30 ms (see Section 6), and the coil currents change by only a few Ampères (i. e., by less than 0.1% for the non-planar coils). It is therefore a good approximation to neglect ($U_{ext\,j} - R_j I_j$), and we obtain

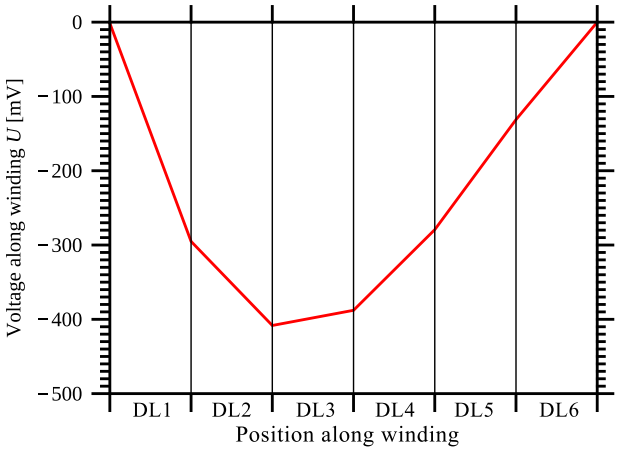

Fig. 10. Voltage along the winding of a type 5 coil during decay of plasma energy with (−420 kJ/30 ms), similar to the end of discharge 20221207.058.

$$0 = -\sum_{k=7}^{7} L_{jk}\frac{\mathrm{d}I_k}{\mathrm{d}t} - \frac{\mathrm{d}\Phi_{\mathrm{dia}\,j}}{\mathrm{d}t} - \frac{\mathrm{d}\Phi_{\mathrm{pc}\,j}}{\mathrm{d}t},$$

where now not the $\mathrm{d}I_k/\mathrm{d}t$ are fixed as in Section 4.2.3, but rather the induced voltages due to the decay of the plasma are prescribed. We therefore have a system of linear equations and can calculate the $\mathrm{d}I_k/\mathrm{d}t$. We then again use Eq. (4) to calculate the voltages across the DLs of a type 5 coil and the QD voltages, resulting in the values listed in Table 4. The graphical representation of the voltage along the winding of a type 5 coil is displayed in Fig. 10. According to our assumption, the power supply just balances the ohmic losses in the normal conducting sections of the circuit, but there is no voltage between the connections to the superconducting part. Due to symmetry in the 10 coils of one type, also the voltage across each single coil must then be 0, and the externally and internally induced voltages must balance within each coil, but they do not balance in each DL. For further illustration, we have also tabulated "term 1" and "term 2" of Eq. (4) separately in Table 4. As can be seen, the resulting voltages across DLs U_{J5} are differences of two large values. The result is therefore sensitive against imprecisions in the calculation of the inductances in the coil system. It is also evident from Table 4 that the input damping factors d are not well adjusted to reduce the U_{QD} values in the fast decay scenario. The d values cannot be chosen to minimise at the same time the voltages during excitation or de-excitation on the one hand side and during changes of the magnetic flux induced by plasma action on the other hand side. In addition, the voltage differences measured in the QDUs depend again sensitively on the d values.

For a first quantitative comparison, the U_{QD} values for coil AAB16 (with the appropriate input damping factors) in the $\mathrm{d}W_{\mathrm{dia}}/\mathrm{d}t$ scenario of Table 4 can now be compared with the maximum measured amplitudes in Fig. 6. The measured voltages can be well explained by our computation, in particular the characteristic pattern of amplitudes when comparing the 4 QD channels of the coil.

4.3. Effect of plasma vessel and coil casing

4.3.1. Model with simplified geometry

For a better assessment of the effects of plasma vessel and coil casing during a fast decay of the plasma energy, we used a model of plasma, plasma vessel, coil casing and 6 DLs with circular geometry (see Fig. 11). The plasma is represented by a cylinder of 0.557 m radius and a length of 3.5 m, its diamagnetism by an azimuthal current of 30 kA. The plasma vessel is represented by a cylinder of 0.89 m radius with the same length as the plasma cylinder. Its wall thickness is the same as for the plasma vessel of W7-X (17 mm), its ohmic resistivity

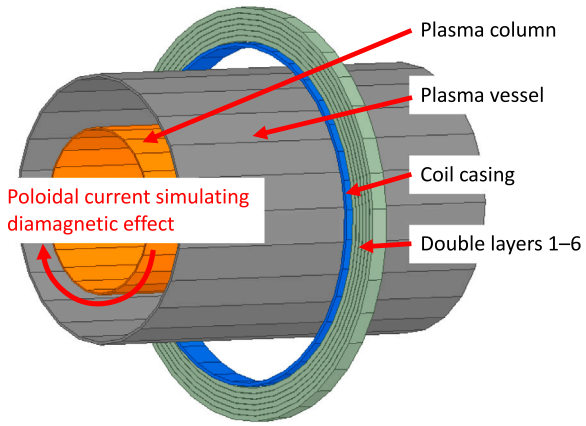

Fig. 11. Geometrically simplified model for electromagnetic analysis (dimensions see text). Only one circular coil is considered. The cross section of the coil casing is condensed as ring (blue) at the inner boundary of the winding double layers. The length of the plasma column with its azimuthal (poloidal) current and plasma vessel is extended in axial direction to keep the major part of the return magnetic flux of the azimuthal current outside the coil.

is $7.2 \cdot 10^{-7}$ Ωm. The 6 DLs are represented by 6 circular layers with the same cross section as the DLs of a non-planar coil (width along the plasma cylinder: 156 mm; thickness: 34 mm; radial separation between the centre lines of adjacent DLs: 36 mm) and 18 windings. The centre line of the entire winding is at a coil radius of 1.187 m. The coil casing is represented by a single layer of 270 mm width and 22 mm thickness with the ohmic resistivity of $5.4 \cdot 10^{-7}$ Ωm (as valid for the stainless steel in use at a temperature of 4 K). This layer is located inside the innermost DL at a radius of 1.055 m, and its cross sectional area is the same as for the entire rectangular hollow coil casing of a non-planar coil (compare Figs. 11 and 1). The time trace of the azimuthal current is derived from the time trace of the diamagnetic energy in discharge 20221207.058 (see Fig. 12). The model is implemented in ANSYS® Electromagnetics Suite (Maxwell 3D) [43]. It can be used to investigate the effect of omitting plasma vessel and coil casing. The voltages thus obtained will be labelled U_{without}.

4.3.2. Resulting QD voltage

In Fig. 13, we compare the resulting voltage across DL 1 with and without the two dissipative components. The damping and delaying effect of plasma vessel and coil casing is clearly visible, although the overall reduction in amplitude is less than 10%. The effect of the plasma vessel is more pronounced than that of the coil casing. In Fig. 14, we compare all 4 QD voltages with and without the damping elements and with the measured voltage in the QD "backup" system. The temporal evolution of the measured signal is very well reproduced by the simulation with plasma vessel and coil casing, however, the amplitude of the simulated signal is too large by a factor of 1.5. This is due to the fact that we used an excessively long section of plasma cylinder to simulate the magnetic flux in the closed torus, with a poloidal current density same as in the full toroidal geometry. A quantitative agreement of the amplitude was therefore not to be expected in this simplified geometry.

4.3.3. Modelling the effect of the dissipative elements

After calculating the induced voltage U_{without} from the current signal of Fig. 12, it is possible to derive a time trace $U_{\mathrm{inside\,coil}}$ approximating the loop voltage signal with plasma vessel and coil casing obtained in the ANSYS® numerical model by convolving the step function U_{without} with the function

$$f(t) = \begin{cases} 0 & t < 0 \\ \frac{1}{\tau}\exp\left(-\frac{t}{\tau}\right) & t \geq 0 \end{cases}: \qquad (7)$$

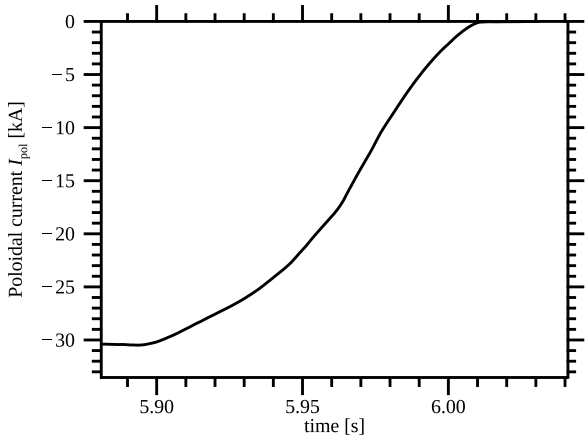

Fig. 12. Temporal evolution of the azimuthal (poloidal) current representing the diamagnetic effect of the plasma as prescribed in the ANSYS® numerical model. The time trace is obtained from the time derivative of the diamagnetic signal of discharge 20221207.058.

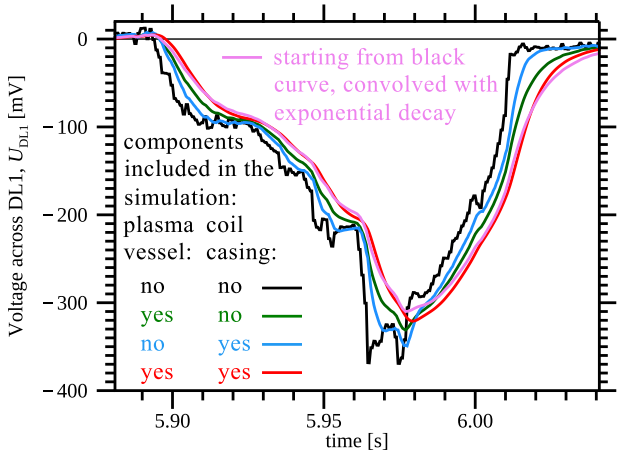

Fig. 13. Resulting voltages across DL1 in the ANSYS® numerical model in response to the change of the azimuthal current in Fig. 12. The results with and without the two dissipative components are shown in different colours. In addition, the convolution of the black curve with an exponential decay ($f(t)$ of Eq. (7) with $\tau = 10\,\mathrm{ms}$) is displayed ($= U_{\text{inside coil}}$).

$$U_{\text{inside coil}} = \int_{-\infty}^{t} U_{\text{without}}(t')\, f(t-t')\, \mathrm{d}t'$$

(see violet curve in Fig. 13). We can then derive from the compensated signal of the diamagnetic loop a single-loop voltage approximating the loop voltage experienced by the field coil windings outside the plasma vessel and inside the coil casing (see Fig. 15). This procedure will be used in the next sections to derive realistic time traces of the voltages induced in the DLs from the linear equations of Section 4.2.

4.4. Quantitative modelling of QD signals and comparison with measured signals

We now compose all information introduced in the previous sections to simulate the expected QD voltages in the QDUs monitoring coil AAB16 in discharge 20221207.058. We start from the $\mathrm{d}\Phi_{\text{dia}}/\mathrm{d}t$ and $\mathrm{d}I_{\text{tor}}/\mathrm{d}t$ signals calculated from the diamagnetic loop and Rogowski coil signals.

These are folded with functions as introduced in Eq. (7) with $\tau_{\text{pol}} = 15\,\mathrm{ms}$ for $\mathrm{d}\Phi_{\text{dia}}/\mathrm{d}t$ and $\tau_{\text{tor}} = 12.5\,\mathrm{ms}$ for $\mathrm{d}I_{\text{tor}}/\mathrm{d}t$ to simulate the damping and delaying effect of the plasma vessel and the coil casing, resulting in dimensionless time traces $f_1(t)$ and $f_2(t)$. (τ_{tor} is

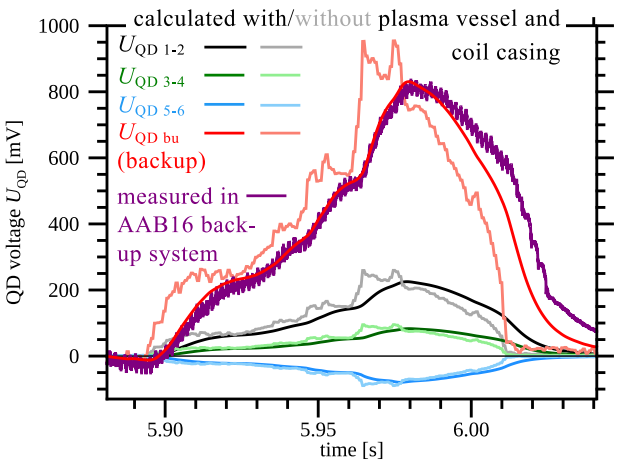

Fig. 14. Resulting QD voltages in the ANSYS® numerical model in response to the change of the azimuthal current in Fig. 12 — comparison of the results without plasma vessel and coil casing (light colours) and with both plasma vessel and coil casing (full colours). For comparison, the measured signal of the AAB16 backup system in discharge 20221207.058, multiplied by 1.5, is added.

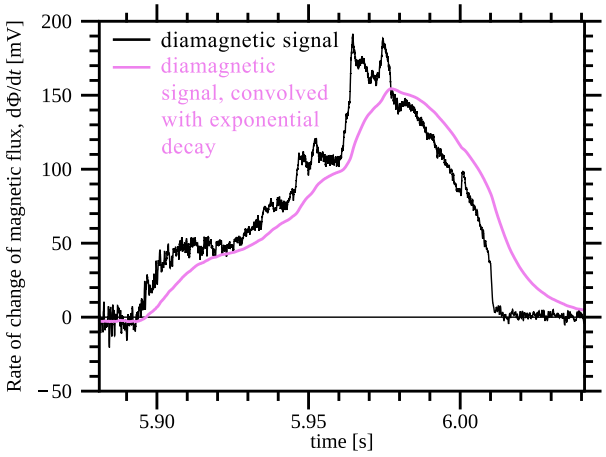

Fig. 15. Application of the filter function of Eq. (7) with $\tau = 10\,\mathrm{ms}$ to the signal of the diamagnetic loop (black). The resulting simulated change in magnetic flux as sensed by a winding outside the plasma vessel and inside the coil casing is shown in violet.

chosen after comparing the signals of a Rogowski coil mounted inside the plasma vessel and a Rogowski coil mounted outside the plasma vessel (see [25]).) We then use the DIAGNO results to scale the signal amplitudes appropriately for the DLs in question. Neglecting the $(U_{\text{ext}\,j} - R_j I_j)$, Eq. (2) can be written

$$\begin{aligned} 0 = &-\sum_{k=1}^{7} L_{jk}(I_{1k} f_1(t) + I_{2k} f_2(t)) \\ &- \sum_{J=1}^{N_{\text{DL}\,j}} n_{\text{wind}\,j}\, \Phi_{\text{dia}\,J\,j}\, f_1(t) \\ &- \sum_{J=1}^{N_{\text{DL}\,j}} n_{\text{wind}\,j}\, \Phi_{\text{pc}\,J\,j}\, f_2(t) \\ &(j = 1, \ldots, 7), \end{aligned} \tag{8}$$

where the $\Phi_{\text{dia}\,J\,j}$ and $\Phi_{\text{pc}\,J\,j}$ are the fluxes through DL J of coil type j due to the plasma diamagnetism and due to plasma currents as calculated by DIAGNO, $N_{\text{DL}\,j}$ is the number of DLs in coil type j, and $n_{\text{wind}\,j}$ is the number of windings per DL in coil type j. Eq. (8) can then be subdivided into two systems of linear equations

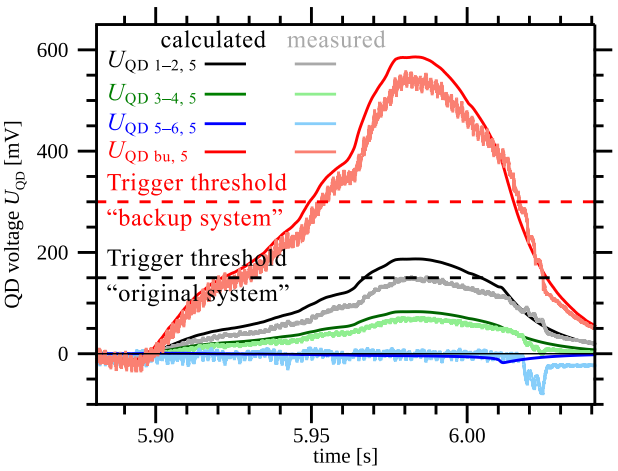

Fig. 16. Comparison between measured QD voltages in coil AAB16 at the end of discharge 20221207.058 (light colours) and calculated QD voltages, using the signals of diamagnetic loop and Rogowski coil to measure plasma energy and toroidal plasma current, respectively, and taking into account the damping and delaying effects of plasma vessel and coil casing as described in Section 4.3.3, plus the set input damping factors d in Eq. (5) for coil AAB16 (full colours).

$$0 = -\sum_{k=1}^{7} L_{jk}\, I_{1k} - n_{\mathrm{wind}\,j} \sum_{J=1}^{N_{\mathrm{DL}\,j}} \Phi_{\mathrm{dia}\,Jj}$$

$$0 = -\sum_{k=1}^{7} L_{jk}\, I_{2k} - n_{\mathrm{wind}\,j} \sum_{J=1}^{N_{\mathrm{DL}\,j}} \Phi_{\mathrm{pc}\,Jj}$$

$$(j = 1, \ldots, 7),$$

which can be solved for the I_{1k} and I_{2k}.

The results can be inserted into Eqs. (4) to obtain the voltages across the DLs and into Eqs. (5) to obtain the QD voltages in the QDUs, taking into account the set damping factors d for the coil in question. This has been done for coil AAB16 at the end of discharge 20221207.058, and the results are compared with the measured QD voltages in Fig. 16. Very good agreement for all four QDUs of this coil is found.

5. Potential modifications of the quench detection system

After analysing the reasons and conditions for triggering the QD system by a fast plasma decay, several ways to avoid this effect can be envisaged. We shall discuss a few options together with their pros and cons in the context of the existing QD system.

5.1. Arrangement of double layers within the winding pack

From the qualitative discussion in Section 4.1.1 it becomes obvious, that the radial stacking of the different DLs within a winding pack, which is reflected by the different inductances of the individual DLs, is a key feature. This results in different induced voltages in the different DLs in response to changes in coil current, irrespective of the origin of such changes (induction caused by changes in the plasma, or excitation or de-excitation by the power supplies). If, instead, the winding layers would be arranged toroidally, at least the induction part due to each coil type's own current would differ significantly less between the DLs of one coil. The differences in the first term on the right hand side of Eq. (6) would therefore be smaller. This would be the pancake winding scheme applied for the toroidal field coils of several superconducting tokamaks (for a discussion of pancake and layer windings see, e. g., [19]). Of course the arrangement of DLs cannot be changed for the existing W7-X device, and there may be prevailing reasons in favour of a radial arrangement of DLs. We shall see that there are further options to cope with the existing design.

5.2. Comparing different pairs of voltages

Instead of comparing voltages across different DLs of the same coil, one could compare voltages across the same DL in different coils of the same type. A survey of the QD voltages measured in different coils of the same type at the end of discharge 20221207.058 shows very similar values of equivalent QD voltages, as it is expected. However, the present design of the QDUs with 3-wire input enforces the comparison of voltages across *electrically adjacent* DLs, since one of the three wires must connect to both DLs (see Section 2.2).

5.3. Changing the sensitivity of the QDUs

The existing QDUs offer three settings to change their sensitivity: (1) the input damping factors d applied to the two input voltages (see Eq. (5)), of which either the first or the second is set to 1 while the other can be set to smaller values; (2) the resistance in the RC circuit determining the integration time of the QD signal; (3) the threshold voltage for the integrated signal to trigger the fast ramp-down of the coil currents. The input damping factors have so far been used to balance the QD voltage to zero for the normal excitation and de-excitation of the coil system. The integration time of the RC circuit and the trigger threshold cannot be set to arbitrarily high values, since the fast ramp-down of the coil currents must be initiated within a limited time period after occurrence of a quench to keep the maximum temperature in the conductor below the specified limit of 130 K [24]. For 2.5 T operation in the next operation phase of W7-X, the integration times and trigger thresholds could nevertheless be changed from (~50 ms, 150 mV) to (~50 ms, 196 mV) for the "original system" and from (~50 ms, 300 mV) to (~100 ms, 333 mV) for the "backup system". For lower field operation, further margins could be used.

5.4. Modifying or replacing the "backup system"

The largest QD voltages during fast changes of Φ_{plasma} occur in the "backup system". However, the redundancy of the QD system should be maintained. It has therefore been suggested to replace the present "backup system" by a second version of the "original system". This does however imply to increase the number of QDUs for the non-planar coils from 4 per coil to 6 per coil.

An inspection of Fig. 10 reveals that the present "backup system" with its central input between DLs 2 and 3 just compares the largest positive and negative voltages available within one coil. A shift to a comparison of the voltages across DLs (1+2+3+4) versus (5+6) would reduce the expected voltages (see Table 5).

5.5. Using external signals to suppress the triggering of the QD system

As shown in Section 4.4, the voltages in the QDUs can be well predicted from the signals of the diamagnetic loop. One could therefore suppress the initiation of a fast ramp-down of the coil currents if at the same time the voltage induced in the diamagnetic loop exceeds an appropriate threshold. This would, however, blind the QD system if at the same time a real quench occurred in one of the field coils. Although the time intervals for which no fast ramp-down could be initiated would be rather short, suggestions of this type were discarded. The same result (delaying the initiation of a fast ramp-down) could by the way be achieved even simpler by further increasing the integration times of the RC circuits within the QDUs.

Table 5
Comparison of the QD voltages in the "backup system" of a type 5 coil for the present setup, comparing the voltage across DLs 1 and 2 with the voltage across DLs 3–6, with an alternative setup, comparing the voltage across DLs 1–4 with the voltage across DLs 5 and 6. The results are shown for the scenarios, (1) coil excitation with 30 A/s, and (2) change of the plasma energy with a rate of (−14 MJ/s) (as in Table 4). For both scenarios, the values are shown both without damping ($d_{bu1} = d_{bu2} = 1$) and with the appropriate damping factor set to 0.5. The alternative setup of the backup system reduces the QD voltage in the reference case with fast plasma decay from 611 mV to 418 mV.

All values in mV	d_{bu1}	d_{bu2}	Coil excitation with 30 A/s	$d\Phi_{dia}/dt \approx +150$ mV
$U_{QD\,bu,\,present} =$	1	1	−1 073	+815
$d_{bu2}\sum_{j=3}^{6} U_{j5} - d_{bu1}(U_{15}+U_{25})$	1	0.5	−105	+611
$U_{QD\,bu,\,alternative} =$	1	1	+844	+557
$d_{bu2}(U_{55}+U_{65}) - d_{bu1}\sum_{j=1}^{4} U_{j5}$	0.5	1	−67	+418

5.6. Using characteristic ratios between QD voltages

For a fixed magnetic configuration, the rates of flux change $d\Phi_{plasma\,Jj}/dt$ in each DL J of a field coil of type j are dominantly fixed multiples of $d\Phi_{dia}/dt$, as determined by the DIAGNO code (see Section 4.2). For short time scales and stationary coil currents, when the $(U_{ext\,j} - R_j I_j)$ terms in Eq. (2) can be neglected, the solution of Eq. (2) will yield dI_k/dt values which are in turn multiples of $d\Phi_{dia}/dt$. The ratio of the voltages across any two DLs U_{Jj} and U_{Kk} of Eq. (4) is therefore only determined by the $(d\Phi_{plasma\,Jj}/dt)/(d\Phi_{dia}/dt)$ and by the self and cross inductances. The same must then be true for the ratios between the different QD voltages. Use of this property of the QD voltages generated by a fast decay of the diamagnetic energy could be made to distinguish voltages due to a fast plasma decay from voltages due to a quench: If the triggering of a fast ramp-down of the coil currents is suppressed if and only if the ratio of the QD voltages detected by different QDUs of one coil is within certain narrow limits, the QD system would not be blinded for real quenches even during a fast plasma decay, since it is most unlikely that simultaneous quenches in several DLs of one coil occur, *which in addition generate voltage differences with ratios in the same narrow range as set in the suppression circuits*. Still, the implementation of such suppression circuits would require a significant modification of the existing QD system.

5.7. Adding voltages at the input of the QDUs

There is a second way to distinguish voltages across the DLs induced by changes in plasma energy and toroidal current from voltages due to a quench. An inspection of Eq. (6) and of Table 4 shows that for damping factors $d \equiv 1$ at least the voltage differences between any two DLs J and K are dominated by the $(L_{DL\,Jjk} - L_{DL\,Kjk})\,dI_k/dt$ terms ("term 1" in Table 4).

If voltages proportional to the dI_k/dt with appropriate amplitudes $L_{DL\,Jjk}$ are added to each DL voltage U_{Jj} of Eq. (4) at the input to each QDU to compensate these inductance terms, only the difference $d\Phi_{plasma\,Jj}/dt - d\Phi_{plasma\,Kj}/dt$ of voltages induced directly by the changes of plasma energy and parallel currents in the two DLs remains in the QD voltage, which is small ("term 2" in Table 4). In addition, the voltage differences between DLs during coil excitation and de-excitation will then also be compensated, which allows to set all damping factors to 1. A similar approach was taken on EAST with the "auxiliary compensation system" to avoid triggering the QD system of the toroidal field coils due to voltages induced from the central solenoid, the poloidal field coils or the toroidal plasma current [44].

Adding the required voltages to the input lines of the QDUs could be done by 7 Rogowski coils around the 7 current leads, picking up the 7 dI_k/dt signals, which would then be distributed to amplifiers at the input of each QDU and coupled to the input lines inductively. At any rate, the QD system itself would require no changes in its logic, no suppression of triggering, no comparison between internal voltages of different QDUs, and it would remain sensitive to any deviations from the expected voltage differences between DLs.

These considerations are valid for the "original system", where a QDU compares the voltages across two adjacent DLs. In the present "backup system" of the non-planar coils, the voltage across 2 DLs is compared with the voltage across 4 DLs. In this case the "term 2" values in Table 4 do no longer almost cancel. The simplest way to correct this would in this case be to modify the backup system into comparing DLs 1–3 with DLs 4–6.

6. Using the field coils to measure the plasma energy

6.1. Motivation

In Section 4.1.1 we outlined that pick-up coils with poloidal winding around the plasma column are a widespread diagnostic to measure changes of the diamagnetic flux Φ_{dia} and to obtain from this the plasma energy. We noted that the field coils of W7-X have the same topology as diamagnetic loops and are therefore also sensitive to changes of Φ_{dia}, which was demonstrated in Section 4. Hence, the idea to use the field coils themselves as diamagnetic loops suggests itself.

Since, as discussed in Section 4.1.1, the voltage induced in a diamagnetic loop is proportional to the *change* of the magnetic flux through the loop, the signal must be integrated to know the diamagnetic energy at any time during a discharge, starting before plasma generation:

$$W_{dia}(t) \propto \int_0^t \frac{d\Phi_{dia}(t')}{dt'}\,dt'$$

with $W_{dia}(0) = 0$. A reliable $W_{dia}(t)$ signal can then be used, e. g., to control an interlock which will switch off plasma heating systems if the plasma energy falls below some threshold. Obviously, any offset voltage will generate an error growing linearly in time. Therefore, a particular effort has been made in the design of the integrating magnetic diagnostics of W7-X and their electronics to avoid sources of offset voltages (e. g., thermovoltages at connectors and electronics offsets) [25,26,45]. Remaining offsets can be measured before the start of the discharge and can be subtracted in real time. After the end of a discharge it can be verified whether $W_{dia}(t)$ has again reverted to 0.

The diamagnetic loops are in addition very sensitive to changes in the vacuum magnetic field, because the magnetic flux through the loop generated by the field coils is much larger than Φ_{dia}. This is why compensation coils are used to determine and to correct for changes of the vacuum magnetic field (see Section 4.1.1). A particular type of error could occur in the measurement of the main diamagnetic loop if its enclosed area changes by a different factor than the area enclosed by the compensation coils. If, e. g., the plasma vessel thermally expands due to a temperature change of 10 K, the change of magnetic flux of the vacuum field through the diamagnetic loop in W7-X with the nominal magnetic field of 2.5 T corresponds to a change of the diamagnetic energy by ~130 kJ. It would therefore be favourable to compare Φ_{dia} measured by the diamagnetic loop inside the plasma vessel with measurements by a loop with well controlled temperature not attached to the plasma vessel [25]. The field coils are such independent loops, operated at a precisely controlled temperature of 4–4.5 K.

The use of the toroidal field coils to measure the diamagnetic energy was indeed already demonstrated for copper coils on the PDX tokamak [46] and on the VEST device [47]. In addition, current and voltage measurements on the superconducting helical windings of the LHD heliotron were used to obtain the diamagnetic energy [48]. Apart from that, measurements of the currents in the helical winding and in the structural shell of LHD were used in conjunction with the voltage induced in a diamagnetic loop to obtain the correct value of the diamagnetic energy [49]. In [46], the author states that the main difficulties were the change of the field coil temperature (with Cu windings) due to ohmic heating and the "nonlinearity and sharp temperature dependence of the resistance of the joints" in the toroidal

field coils. Both effects do not play a role in the W7-X superconducting field coils — this is corroborated by the successful application of the idea in LHD [48].

In this Section 6 we shall use the signals of the existing current and voltage measurements of the field coils to investigate how well $W_{\mathrm{dia}}(t)$ and $I_{\mathrm{tor}}(t)$ can be derived from these signals on W7-X. We cannot expect to obtain the same time resolution as from the diamagnetic loop and the Rogowski coil inside the plasma vessel, due to the shielding by eddy currents in the plasma vessel and coil casings. As explained above, our main interest is in the behaviour of the signals in "long" discharges, where we are sensitive to offset drifts in the electronics. We are aware, that the electronics measuring the voltages applied to the coil circuits have so far not been optimised for low offset drifts like those of the equilibrium magnetic diagnostics.

The results of the DIAGNO code show that the magnetic flux due to plasma currents Φ_{pc} in comparison with Φ_{dia} is larger for the non-planar field coils than for the diamagnetic loop (see Table 2). Therefore, two different types of field coils may have to be used to disentangle the effects of $\mathrm{d}\Phi_{\mathrm{dia}}/\mathrm{d}t$ and of $\mathrm{d}I_{\mathrm{tor}}/\mathrm{d}t$.

In order to assess how well the idea works to use the field coils as diamagnetic loops, we shall first analyse which signals can be used to derive Φ_{dia} (and possibly I_{tor}) from the field coils in Section 6.2. We shall then compare the results between the diamagnetic loop and the field coils for fast changes of Φ_{dia} in Section 6.3 and finally add a comparison for entire discharges in Section 6.4, including one "long" discharge and the discussion how to assess the impact of offset drifts. We shall discuss the results in Section 7.2.

6.2. Required and available measurements

From the equations introduced in Section 4.2 we find two options to learn about $\mathrm{d}\Phi_{\mathrm{plasma}}/\mathrm{d}t$ through the field coils. As a first option, using Eq. (2) requires the measurement of the applied voltage to the field coils of type j, $U_{\mathrm{ext}\,j}$, and of all 7 field coil currents, I_k. In addition, the inductance matrix of the 7 coil circuits (L_{jk}) must be known. The $U_{\mathrm{ext}\,j}$ and I_k are constantly recorded with a sample rate of 1 kHz during the operation of the coil system. This option can be used in any toroidal magnetic confinement device.

Alternatively, Eq. (4) can be used as the second option, which requires the measurement of the voltage U_{Jj} across one or several DLs J of coil type j and again all 7 field coil currents I_k. This is possible in W7-X, where the windings of each superconducting field coil are tapped by QD wires at the DL connectors. Presently, the U_{Jj} are not measured directly, but certain differences U_{QD} between them (see Eqs. (5)–(6)) are recorded during an interval of 10 s around the triggering of the QD system data storage (see Section 2.2). In these differences, only the small differences between the induced voltages $\Phi_{\mathrm{plasma}\,\{J\}j}$ in the different DLs $\{J\}$ of a fixed coil type j remain, possibly enlarged by the difference of the damping factors $d_{\{J\}}$.

For the distinction between Φ_{dia} and Φ_{pc} of Eq. (3), we assume for the plasma-generated magnetic flux through coil circuit j

$$\Phi_{\mathrm{plasma}\,j} = g_j W_{\mathrm{dia}} + h_j I_{\mathrm{tor}}, \tag{9}$$

where W_{dia} is the diamagnetic energy measured by the main diamagnetic loop, and I_{tor} is the net toroidal plasma current measured by a Rogowski coil. The g_j and h_j are determined from model equilibria with the DIAGNO code (see Section 4.1.2). The DIAGNO code shows additional dependencies of $\Phi_{\mathrm{plasma}\,j}$ on W^2 and on the radial profile shapes of plasma pressure and toroidal current density, but these dependencies are very weak and will be neglected here.

Likewise, we assume for the plasma-generated flux through DL J of coil type j

$$\Phi_{\mathrm{plasma}\,Jj} = g_{Jj} W_{\mathrm{dia}} + h_{Jj} I_{\mathrm{tor}}. \tag{10}$$

Table 2 can be used to obtain the g_j and h_j for the 7 coil circuits and the g_{Jj} and h_{Jj} for the innermost and outermost DLs. According to the values in this table, of the non-planar coil circuits, the type 1 coil circuit is most sensitive to changes in W_{dia} and least sensitive to changes in I_{tor}, whereas the type 3 and 4 circuits are least sensitive to changes in W_{dia} and most sensitive to changes in I_{tor}.

Using the first option, from Eqs. (2) and (9) for two different circuits j and l we then obtain

$$\frac{\mathrm{d}W_{\mathrm{dia}}}{\mathrm{d}t} = \frac{h_l(U_{\mathrm{ext}\,j} - R_j I_j) - h_j(U_{\mathrm{ext}\,l} - R_l I_l) - \sum_{k=1}^{7}(h_l L_{jk} - h_j L_{lk})\frac{\mathrm{d}I_k}{\mathrm{d}t}}{g_j h_l - g_l h_j} \tag{11}$$

$$\frac{\mathrm{d}I_{\mathrm{tor}}}{\mathrm{d}t} = \frac{g_l(U_{\mathrm{ext}\,j} - R_j I_j) - g_j(U_{\mathrm{ext}\,l} - R_l I_l) - \sum_{k=1}^{7}(g_l L_{jk} - g_j L_{lk})\frac{\mathrm{d}I_k}{\mathrm{d}t}}{h_j g_l - h_l g_j}. \tag{12}$$

Likewise, for the second option, from Eqs. (4) and (10) for two different DLs J and K of the same coil type or of two different coil types j and l we obtain

$$\frac{\mathrm{d}W_{\mathrm{dia}}}{\mathrm{d}t} = -\frac{h_{Kl}U_{Jj} - h_{Jj}U_{Kl} + \sum_{k=1}^{7}(h_{Kl}L_{\mathrm{DL}\,Jjk} - h_{Jj}L_{\mathrm{DL}\,Klk})\frac{\mathrm{d}I_k}{\mathrm{d}t}}{g_{Jj}h_{Kl} - g_{Kl}h_{Jj}} \tag{13}$$

$$\frac{\mathrm{d}I_{\mathrm{tor}}}{\mathrm{d}t} = -\frac{g_{Kl}U_{Jj} - g_{Jj}U_{Kl} + \sum_{k=1}^{7}(g_{Kl}L_{\mathrm{DL}\,Jjk} - g_{Jj}L_{\mathrm{DL}\,Klk})\frac{\mathrm{d}I_k}{\mathrm{d}t}}{h_{Jj}g_{Kl} - h_{Kl}g_{Jj}}, \tag{14}$$

and similar expressions can be derived from the QD voltages, Eq. (6), including the individual damping factors. To reduce the impact of uncertainties in the measurements and in the derivation of the cross inductances and the g and h factors, combinations (j,l), (J,j,K,l), or the corresponding combination for Eq. (6) should be chosen such as to maximise the respective denominators $(g_j h_l - g_l h_j)$ etc. In order to distinguish the diamagnetic energy and toroidal plasma current calculated from the field coil signals according to Eqs. (11)–(14) from the values obtained from diamagnetic loop and Rogowski coil, we shall mark them with additional subscripts 'fc1' (for Eqs. (11)–(12)) and 'fc2' (for Eqs. (13)–(14)).

In the end, the computation of W_{dia} and I_{tor} always requires an integration in time either of the voltages measured at the power supplies of the coil circuits $U_{\mathrm{ext}\,j}$ or of the QD voltages. In order to minimise the impact of offsets originating in electronics and data acquisition, offsets and linear trends of the integrated signals are determined before the start and after the end of the plasma discharge. This is discussed in more detail in Section 6.4.3. In the case of the $U_{\mathrm{ext}\,j}$ this includes the offset to drive the constant coil current I_{j0} across the remaining ohmic resistance R_j (mainly due to the aluminium current leads between power supply and superconducting part of the circuit). If I_j deviates from I_{j0} during the discharge, the $\int^t R_j(I_j(t) - I_{j0})\,\mathrm{d}t'$ term must be taken into account in the integration to obtain correct results for $W_{\mathrm{dia,fc}}(t)$ and $I_{\mathrm{tor,fc}}(t)$. The measured values of R_j for the 7 coil circuits are used for this purpose.

In practice, the use of Eqs. (9)–(14) implies the computation of a further layer of differences between quantities of almost the same size. This is a challenge with the existing signals, since in particular several of the coil current signals I_k exhibit high noise levels. On the other hand side, an inspection of Table 2 shows that, for typical plasma energies W_{dia} and toroidal plasma currents I_{tor} in W7-X, the contribution of I_{tor} to Φ_{plasma} is still small even for the field coils. We shall therefore in the following sections assume the following relations instead of Eqs. (9)–(14):

$$\Phi_{\mathrm{plasma}\,j} = g_j W_{\mathrm{dia}} \tag{15}$$

$$\Phi_{\mathrm{plasma}\,Jj} = g_{Jj} W_{\mathrm{dia}} \tag{16}$$

Hence,

$$\frac{\mathrm{d}W_{\mathrm{dia,fc3}}}{\mathrm{d}t} = \frac{U_{\mathrm{ext}\,j} - R_j I_j - \sum_{k=1}^{7} L_{jk}\frac{\mathrm{d}I_k}{\mathrm{d}t}}{g_j} \tag{17}$$

$$\frac{\mathrm{d}W_{\mathrm{dia,fc4}}}{\mathrm{d}t} = -\frac{U_{Jj} + \sum_{k=1}^{7} L_{\mathrm{DL}\,Jjk}\frac{\mathrm{d}I_k}{\mathrm{d}t}}{g_{Jj}}. \tag{18}$$

We shall revisit the influence of the plasma current in Section 6.4.2.

6.3. Comparison between magnetic diagnostics and field coil signals for short time scales

We consider the fast plasma decay at the end of discharge 20221207.058. We have already compared the QD voltages to be expected in coil AAB16 with the measured signals in Section 4.4 (see Fig. 16), and found fair agreement. We shall now extend our comparison to include the changes in the *measured* coil currents in Eq. (4) rather than deriving them from Eq. (2) under the assumption $U_{\mathrm{ext}\,j} - R_j I_j \equiv 0$, and to using the QD signals of more than just a single coil. We shall further use the coil currents and the voltages at the power supplies of the coil circuits as an alternative way to calculate the diamagnetic energy (using Eq. (17)).

In this discharge, the toroidal plasma current was very small. Its neglect (i. e., using Eqs. (17) and (18) rather than (11) and (13)) seems therefore justified.

We only consider the time interval [5.83 s, 6.07 s]. The voltages of the coil circuit power supplies $U_{\mathrm{ext}\,j}$ and the coil currents I_k in Eq. (17) are only available up to ~6.02 s. After this time, the coil circuits are temporarily closed through current breakers bridging the power supplies, and the power supplies are then disconnected, before the current path through the dump resistors is established and the fast ramp-down of the coil currents begins. The QD voltages are longer available, but the current signals are missing for the use of Eq. (18). A zero level after the discharge can therefore not be determined for $W_{\mathrm{dia,\,fc}}$ with either method. This is why we shift each of the $W_{\mathrm{dia,\,fc}}$ signals determined from Eq. (17) or (18), such that its average in the interval [5.85 s, 5.88 s] is equal to the average of the compensated W_{dia} signal from the diamagnetic loop (which we shall abbreviate as 'CWdia' in our further discussion).

The results are shown in Fig. 17: In addition to the CWdia signal (black curve), the version of CWdia taking into account the damping and delaying effects of plasma vessel and coil casing (as described in Section 4.3.3) is displayed (grey curve). The $W_{\mathrm{dia,\,fc}}$ traces derived from the field coil signals should be compared with this grey curve. The seven $W_{\mathrm{dia,\,fc3}}$ curves of Eq. (17) exhibit significant noise in spite of the application of a running average over 10 ms. The noise level is, however, different for the different coil circuits. It is lowest for the coils of types 4, 5 and B (blue, dark blue and dark magenta curves).

When using the QD voltages (according to Eq. (18), where weighted differences between the U_{Jj} must be used to obtain the measured voltages U_{QD} of Eq. (5)), 200 different QD signals from the non-planar coils are available. For the purpose of calculating the induced voltage in each DL, it would of course be preferable to record the voltages across the DLs, U_{Jj}, themselves rather than the weighted differences U_{QD}. Indeed, the 200 $W_{\mathrm{dia,\,fc4}}$ signals thus derived have very different quality. The $U_{\mathrm{QD\,3-4}}$ and $U_{\mathrm{QD\,5-6}}$ are mostly unusable, the $U_{\mathrm{QD\,1-2}}$ are better, and the signals from the "backup system" $U_{\mathrm{QD}\,bu}$ perform best, but still show large differences between the different coil types or even between the coils of same type. Most probably this is due to the imperfect knowledge of the damping factors d of Eq. (5). We found rather good agreement with the filtered CWdia signal when averaging over the $U_{\mathrm{QD}\,bu}$ signals of all ten type 4 or type 5 coils (green and red curves in Fig. 17).

In Fig. 18, we display separately the two contributions to $W_{\mathrm{dia,\,fc}}$ in Eqs. (17) and (18). On this time scale of order 100 ms, the coil currents follow the change in diamagnetic energy immediately (only delayed by the eddy currents in plasma vessel and coil casing) to maintain the magnetic flux (cyan and light green/magenta curves). The voltage in the power supplies (blue curves) is not reacting to the changes of the coil currents on this short time scale. While the main contribution in Eq. (17) is due to the changes in coil currents, the main contribution in Eq. (18) is due to the QD voltages, which are reflecting the changes in coil currents.

After all, on the 50–200 ms time scale, the $W_{\mathrm{dia,\,fc}}$ curves determined from both Eqs. (17) and (18) agree fairly well with the CWdia signal,

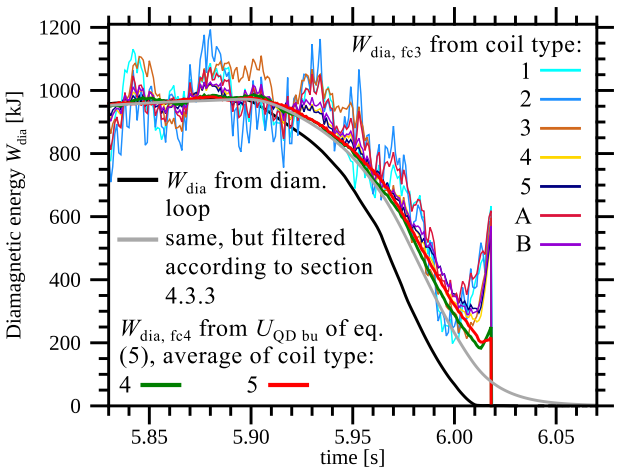

Fig. 17. Diamagnetic energy at the end of discharge 20221207.058 derived from currents and voltages of the field coil circuits, compared with the result from the compensated diamagnetic loop. The signals derived from the field coil circuits are only available up to $t \sim 6.02$ s, since at this time the coil circuits are disconnected from the power supplies to commute the currents into the dump resistors for fast shutdown. Hence, it is not possible to determine a 0 level at the end of the discharge. Instead, the signals are shifted as described in the text. The cyan/blue/violet curves are from $U_{\mathrm{ext}\,j}$ and I_j according to Eq. (17). The $W_{\mathrm{dia,\,fc3}}$ traces for the different coil types j are shown to demonstrate the range of results and noise levels. The green and red curves are from the average of the values calculated from the QD voltages of the "backup system" of all type 4 or type 5 coils and from the coil currents according to Eq. (18). Since the coils are outside the vacuum vessel, there signals should be compared with the filtered version of the diamagnetic coil signal as described in Section 4.3.3 (grey) rather than with the black curve itself.

if the dissipative effects of plasma vessel and coil casing are taken into account. However, the coil current signals partly exhibit unpleasantly high noise levels, and the uncertainty in the damping factors of the QD system requires the selection of usable channels and averaging over these channels. The time integration of the voltage signals is sufficiently short, such that offset drifts play no role.

6.4. Comparison between magnetic diagnostics and field coil signals for long time scales

6.4.1. Without consideration of toroidal plasma current

Next, we compare the $W_{\mathrm{dia,\,fc}}$ and CWdia signals for two entire discharges. In neither of them a fast ramp-down of the coil currents was initiated. Both discharges were in magnetic "standard" configuration. The CWdia and the toroidal plasma current measured by a Rogowski coil are shown in Fig. 19. Discharge 20230126.070 was a very short discharge. In this discharge, the data storage of the QD system was triggered manually around the end of the discharge, and this is the only case where the QD voltages were recorded during the entire length of a plasma discharge, such that offset corrections are possible before plasma start-up and after the end of the plasma. In contrast, 20230215.032 has been one of the longest W7-X discharges so far and serves to compare the long-term behaviour between the $W_{\mathrm{dia,\,fc3}}$ and CWdia signals. For this discharge, no QD signals are available.

In Figs. 20 and 21, we show the same signals for discharge 20230126.070 as in Figs. 17 and 18 for the end of discharge 20221207.058, and the colour code is the same. Only the grey curve of Fig. 17, representing the CWdia signal with the dissipative effects of plasma vessel and coil casing, is omitted here, since it is indistinguishable from the black curve on the time scale of Figs. 20 and 21. Again, we find good agreement between the $W_{\mathrm{dia,\,fc}}$ and the CWdia signals. The separate representation in Fig. 21 of the different contributions in Eqs. (17) and (18) shows how the current control of the field coil circuits modifies the voltages of the power supplies to restore the coil

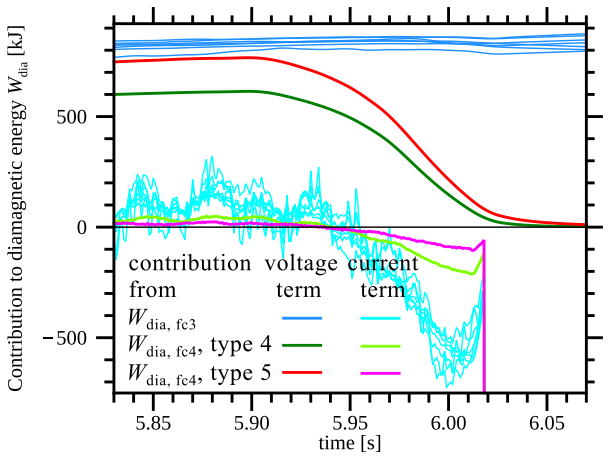

Fig. 18. Separate representation of the voltage and current terms of Eq. (17) to $W_{dia,fc3}$ and of Eq. (18) to $W_{dia,fc4}$ for the signals shown in Fig. 17: For Eq. (17), the contributions of the current terms ($\sum_{k=1}^{7} L_{jk} I_k$) and of the voltage terms ($-\int (U_{ext\,j} - R_j I_j) dt$) are drawn in the same colour for all circuits j; they are shown to demonstrate the range of results and noise levels. For Eq. (18), the contributions of the measured QD voltages (voltage term) and the contributions of the changes in coil currents (current term) are again shown for the "backup system" averaged over the type 4 or the type 5 coils. The signal of the diamagnetic loop is not shown in this figure.

currents to the set values on the time scale of ~1 s (see discussion in figure caption). The high noise level of the field coil current signals is again visible, although a running average over 50 ms was calculated for these figures.

For the 480 s discharge 20230215.032, we display the $W_{dia,fc3}$ signals together with the CWdia signal in Fig. 22. A characteristic time of order several 10 s becomes visible in the signals derived from the field coil currents and voltages: The toroidal plasma current can no longer be neglected in this discharge (see Fig. 19), and we observe its coupling to the field coils (compare the coupling constants in Table 2, which were calculated using the DIAGNO code). Note in particular that this coupling is not as visible in the curve of the type A coil circuit (violet), in qualitative agreement with the predictions of the DIAGNO code, in which the coupling is smaller and with reversed sign for the type A planar coils. Although running averages over 1 s are displayed in this figure, we note again the different but high noise level in the coil current signals, which is lowest for the type 4 and type 5 circuits.

In Fig. 23, we display the disintegration into the voltage and current terms in Eq. (17) only for the type 5 and type A coil circuits, together with the complete signals already known from Fig. 22. On this long time scale, the deviations of the coil currents (smoothed again over 1 s) are hardly visible above the noise (cyan and orange curves), since the deviations from their set values are adjusted to 0 by the coil current control. Almost the entire information on the flux changes due to the diamagnetic effect and due to plasma currents is contained in the integrated voltage signals. A 10 s interval around the plasma start-up is enlarged for the type 5 coil signals in Fig. 24. Here, the quick rise of the coil currents (cyan) on the time scale of the diamagnetic energy (black) is clearly visible. The voltage of the power supply (light blue) then reacts and brings the coil current back down to its set value, with a slight overshoot. The combination of the signals (dark blue) reproduces well the diamagnetic energy signal. The influence of the toroidal plasma current is not yet visible in this time interval, since it takes about 30–40 s (typical L/R time for I_{tor} in W7-X) before I_{tor} reaches its equilibrium level of 8–10 kA (see Fig. 19).

6.4.2. With consideration of toroidal plasma current

Since the influence of I_{tor} is clearly visible in the $W_{dia,fc3}$ signals for discharge 20230215.032, but a disentanglement of W_{dia} and I_{tor} according to Eqs. (11) and (12) does not yield satisfactory results (see Section 6.2), we now choose a different approach to quantify the impact of I_{tor} on the field coil signals. Rather than using Eqs. (11)–(12) to determine $W_{dia,fc1}$ and $I_{tor,fc1}$ from two different field coil circuits with the g and h coefficients obtained from DIAGNO, we shall now use the obvious difference in the time behaviour of W_{dia} and I_{tor} visible in Fig. 19 to express $\Phi_{plasma\,j}$ of Eq. (2) as linear combination of the CWdia signal and the I_{tor} signal from the Rogowski coil:

$$M_j \equiv \int_0^{t_{end}} \left[\left(\int^t (U_{ext\,j} - R_j I_j)\, dt' - \sum_{k=1}^{7} L_{jk} I_k(t) \right) - \left(g_{fit\,j}\, W_{dia}(t) + h_{fit\,j}\, I_{tor}(t) \right) \right]^2 , \quad (19)$$

where the first expression on the right hand side is offset corrected, and the $g_{fit\,j}$ and $h_{fit\,j}$ are fit parameters obtained by minimising M_j from the time traces of discharge 20230215.032. In Table 6 we have tabulated the resulting fit parameters, which can be compared with the values in Table 2 calculated from DIAGNO simulations. In Fig. 25, a comparison between the two expressions on the right hand side of Eq. (19) is shown for four coil circuits j. We find that the qualitative behaviour of $\Phi_{plasma\,j}(t)$, with transients on the time scale of several 10 s after the changes of the heating power, can be well reproduced by adding an $I_{tor}(t)$ contribution to the $W_{dia}(t)$ signal. The fitted g values of Table 6 agree rather well with the values obtained with the DIAGNO code of Table 2, while the deviations in the h values are larger for a number of coil types. The time traces of the fitted curves (green in Fig. 25) do reproduce the $\Phi_{plasma\,j}(t)$ (black curves) well in most cases, although there are a few deviations in detail.

One should note that the use of Eq. (2) to obtain $\Phi_{plasma\,j}(t)$ requires the time integration of $(U_{ext\,j} - R_j I_j)$, which is sensitive to offsets and offset drifts. The particular algorithm for offset and drift correction we used is described in the following section, which uses the drifts in the $\Phi_{plasma\,j}(t)$ signals before the start and after the end of the plasma discharge (when the $\Phi_{plasma\,j}$ should be $\equiv 0$). The values of the $g_{fit\,j}$ and $h_{fit\,j}$ and the fit quality resulting from Eq. (19) sensitively depend on the offset and drift correction algorithm used.

Table 6
Fit parameters $g_{fit\,j}$ and $h_{fit\,j}$ of Eq. (19) to describe the time traces of the single-loop magnetic fluxes $\Phi_{plasma\,j}$ from Eq. (2) in discharge 20230215.032 as linear combinations of $W_{dia}(t)$ and $I_{tor}(t)$ as measured by diamagnetic loop and Rogowski coil. The results for all 7 coil circuits $j = 1,\ldots,7$ are given. For better comparability, $g_{fit\,j}$ and $h_{fit\,j}$ are given in the same units as g_j and h_j obtained from the DIAGNO code in Table 2. While the $g_{fit\,j}$ mostly agree fairly well with the g_j, the differences are relatively larger between $h_{fit\,j}$ and h_j. In Fig. 25 we show the time traces for four of the seven coil circuits as examples for good and for not as good agreement.

	Field coil type j						
	1	2	3	4	5	A (= 6)	B (= 7)
$g_{fit\,j}$ [mVs/MJ]	−10.3	−10.3	−9.3	−8.8	−9.2	−12.3	−8.3
$h_{fit\,j}$ [mVs/(10 kA)]	+1.31	+1.37	+1.48	+1.07	+0.80	+0.21	+1.03

6.4.3. Assessing drifts in the time integrals

All time traces presented so far, which involved the integration in time of experimental signals, were corrected for drifts. This applies to the CWdia signal and the I_{tor} signal from the Rogowski coil as well as for the $W_{dia,fc}$ signals. The correction is based on the fact that without plasma Φ_{plasma} must be 0. Regression lines to the $\Phi_{plasma}(t)$ signals obtained from experimental data are therefore calculated in a time interval before the start of the plasma and in a time interval after the end of the plasma discharge (if usable data are available in these time intervals). Ideally, both regression lines will agree, and we would then be confident that the same drift prevails during the entire plasma discharge and just subtract this regression line from the calculated Φ_{plasma} signal. For a long discharge like 20230215.032, however, usually the two regression lines will not agree, neither in their offset nor in their slope. This is shown in Fig. 26 for the CWdia signal and for

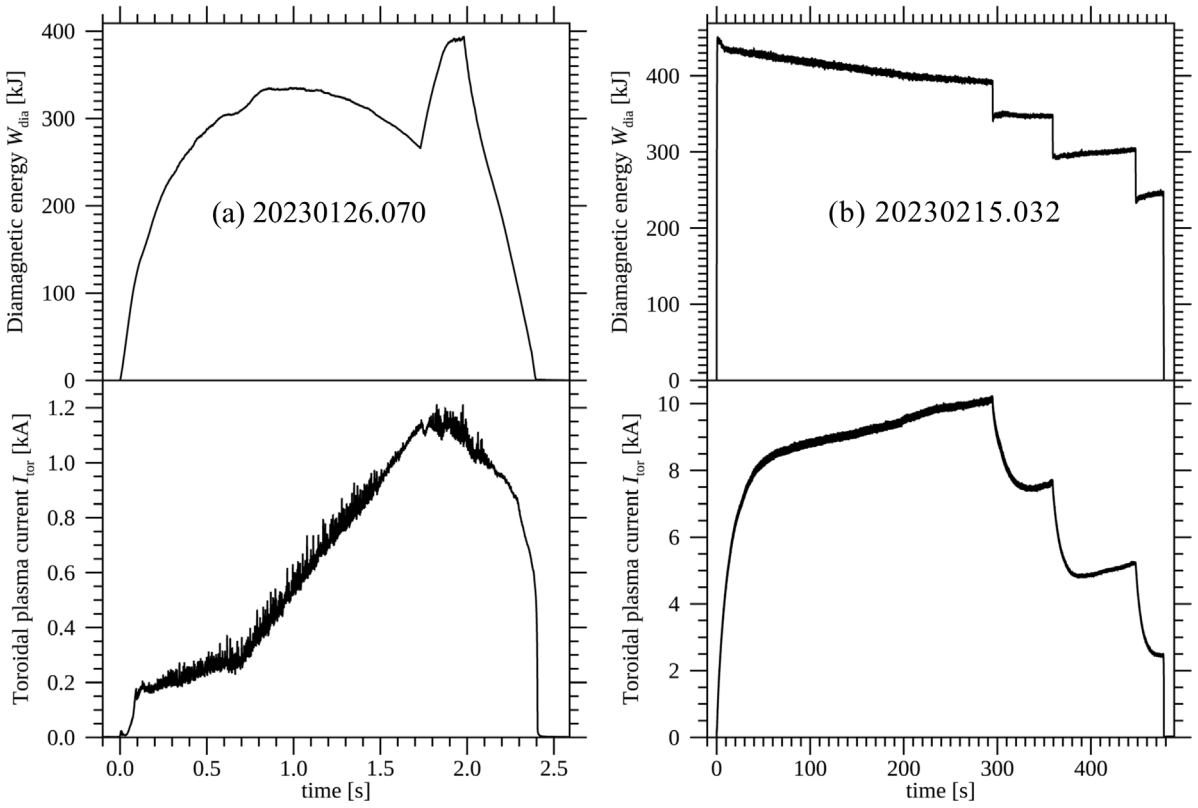

Fig. 19. W_{dia} and I_{tor} as measured with the diamagnetic loop and the Rogowski coil during discharges 20230126.070 and 20230215.032. For these two discharges, we shall compare the diamagnetic energy as derived from the currents and voltages in the field coil circuits with the time traces shown here. In discharge 20230215.032, several gyrotrons switched off successively, and the quick response of W_{dia} and slower response of I_{tor} (bootstrap current) due to the long L/R time for toroidal plasma currents in W7-X is nicely visible.

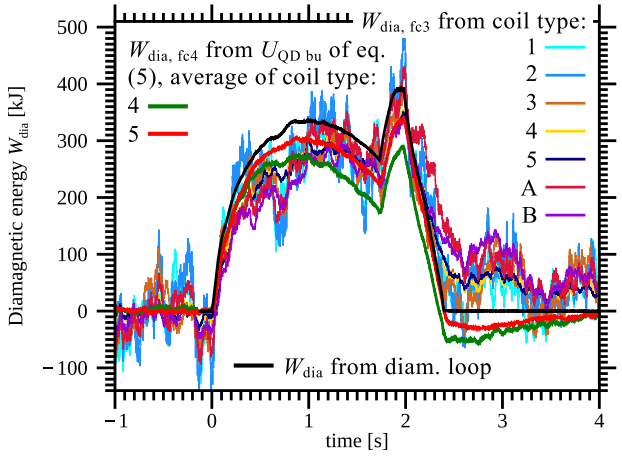

Fig. 20. Diamagnetic energy during discharge 20230126.070 derived from currents and voltages of the field coil circuits, compared with the result from the compensated diamagnetic loop (black). In this discharge, the data acquisition of the QD system was triggered manually, and the discharge is sufficiently short such that QD system data encompass the plasma start-up as well as the plasma end. An offset and drift compensation for the QD signals could therefore be performed same as for the coil circuit voltages. Like in Fig. 17, the $W_{dia, fc3}$ traces for the different coil types j are only shown to demonstrate the range of results and noise levels.

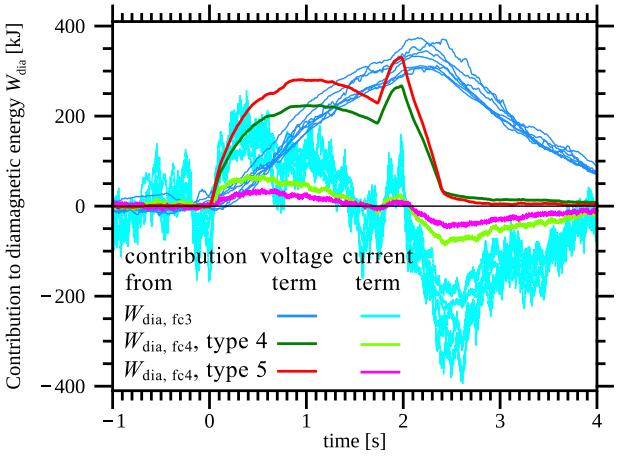

Fig. 21. Separate representation of the voltage and current terms of Eqs. (17) and (18) for the $W_{dia, fc}$ signals shown in Fig. 20. On this time scale of a few seconds, we observe first the coil current terms to increase in inductive response to the reduction of flux due to the build-up of diamagnetic energy at plasma start-up. The voltages of the power supplies then respond (shown here in blue are the integrated voltages with a negative sign, corresponding to the first term in Eq. (17)) to bring the coil currents back down to the set values. This takes about 1–2 s, but then the plasma discharge is over, the plasma energy reverts to 0, and the entire response of the coil circuits repeats with reversed sign. The terms contributing to $W_{dia, fc3}$ for the different coil circuits j are all shown in the same colours, only to demonstrate the range of results in the different circuits.

five of the seven $W_{dia, fc3}$ signals calculated from the field coil circuit voltages and currents. We have no information about the evolution of the error signal to be subtracted during the plasma discharge. We therefore assume a smooth transition between the two regression lines, which is achieved by calculating a cubic spline between the two time intervals in which the regression lines are determined (green curves in Fig. 26). These green curves were subtracted from the W_{dia} signals to obtain the curves presented in the previous sections. We emphasise

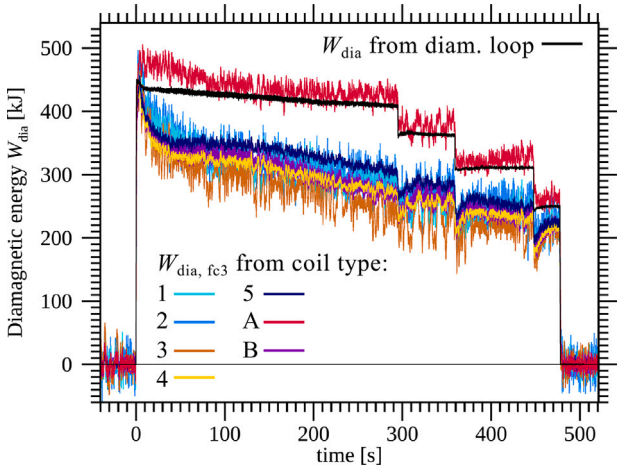

Fig. 22. Diamagnetic energy during discharge 20230215.032 derived from currents and voltages of the field coil circuits, compared with the result from the compensated diamagnetic loop.

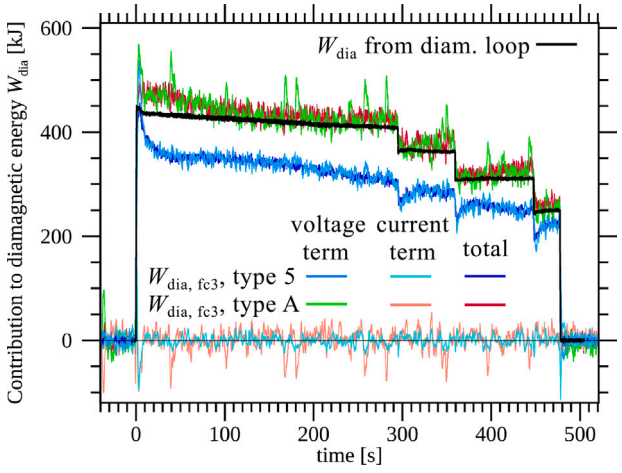

Fig. 23. Separate representation of the voltage and current terms of Eq. (17) for the $W_{dia, fc3}$ signals shown in Fig. 22 for coil circuits 5 and A. We display the total $W_{dia, fc3}$ signal, the $(\sum_{k=1}^{7} L_{jk} I_k)$ term ("current term") and the $(-\int (U_{ext\,j} - R_j I_j) dt)$ term ("voltage term") together with the CWdia signal.

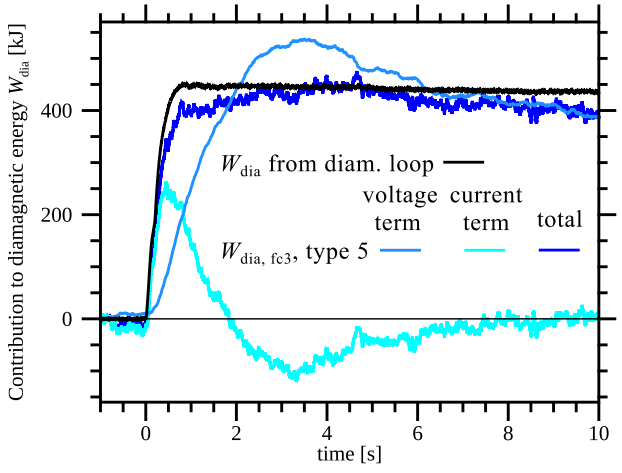

Fig. 24. Separate representation of the voltage and current terms of Eq. (17) for the $W_{dia, fc3}$ signal derived from the type 5 coil circuit during the first 10 s of discharge 20230215.032. The coil current signals are smoothed here over 50 ms.

again that the agreement between the different $W_{dia, fc}$ signals and the values of the fit parameters $g_{fit\,j}$ and $h_{fit\,j}$ depend on this drift correction algorithm. In particular, the $h_{fit\,j}$ are rather sensitive to changes in the algorithm.

Our main argument for the use of the field coils as diamagnetic loops was the confidence that the plasma-generated magnetic flux through their windings might be less affected by perturbing influences like thermal expansion. At the same time, the measurements should not be jeopardised by other offset drifts, which become visible as deviations between the regression lines before and after the plasma interval. We quantify this deviation by the offset of the magenta line from the orange line at the end of the plasma (ΔW_{dia}) and by the difference in their slopes $\Delta b_{regress}$. These two quantities are compared between the CWdia signal and the $W_{dia, fc3}$ signals in Table 7. In terms of these quantities, we find that most of the $W_{dia, fc3}$ signals perform worse than the CWdia signal. On the other hand side, considering that the electronics of the field coil circuits were not designed for long-time integration like those of the magnetic diagnostics, the results are promising and might be worth further investigation, in which the specialised electronics under use for the equilibrium magnetic diagnostics should be employed to record $U_{ext\,j}$ signals or DL voltages.

7. Discussion

7.1. Voltages in the QD system during changes of the plasma-generated magnetic flux

Unusually fast changes (decays) of plasma energy in W7-X did trigger the QD system of the superconducting field coils, resulting in fast ramp-downs of the coil currents and, subsequently, an interruption of experiments for at least several hours. It was known that there is an inductive interaction between the plasma energy and the field coils due to the plasma diamagnetism (in the context of measurement or correction of the diamagnetic energy [25,46–49] and also in the context of quench detection, e. g. [13]). Nevertheless, such an effect on the W7-X QD system was unexpected. In contrast to most superconducting tokamaks, where the toroidal field coil windings consist of toroidally stacked pancakes or double pancakes (see, e. g., [10,13,14,19,20]), the W7-X field coil windings are formed by radially stacked double layers. In addition, whereas in the QD systems of other devices the voltages across entire toroidal field coils or across equivalent (double) pancakes are compared (see, e. g., [10,11,13,14]), or the voltage is measured on co-wound wires rather than on the winding itself [12], the W7-X QD system compares voltages across different DLs of the same coil. Whereas the directly induced voltages due to changes of the diamagnetic energy are still quite close to each other in the different DLs, the voltages induced due to changes of the coil currents differ by larger amounts (see Table 4), since the inductances of adjacent DLs differ by up to 5–10% (see Table 3).

We have qualitatively explained this effect in Section 4.1 and have then quantitatively analysed the interaction between plasma and coil system and calculated the expected voltages in the QD system, and we have demonstrated that our modelling well reproduces the measured voltage signals (see Section 4.4). The model reveals that the differences in voltage between adjacent double layers of the field coil windings, which are used by the QD system, depend on small differences between large values: In the example discussed in Section 4, the voltages across double layers of order 100–200 mV result as differences between the externally induced voltages and the voltages induced by changes of the coil currents, both of order 2 000 mV (see Table 4), and the differences between self and cross inductances of adjacent double layers with the other windings of the field coil system are below 5–10% of their absolute values (see Table 3). In particular, these differences and the true damping of input voltages in the QD units must be precisely known to predict the voltages deciding on the triggering of the QD system.

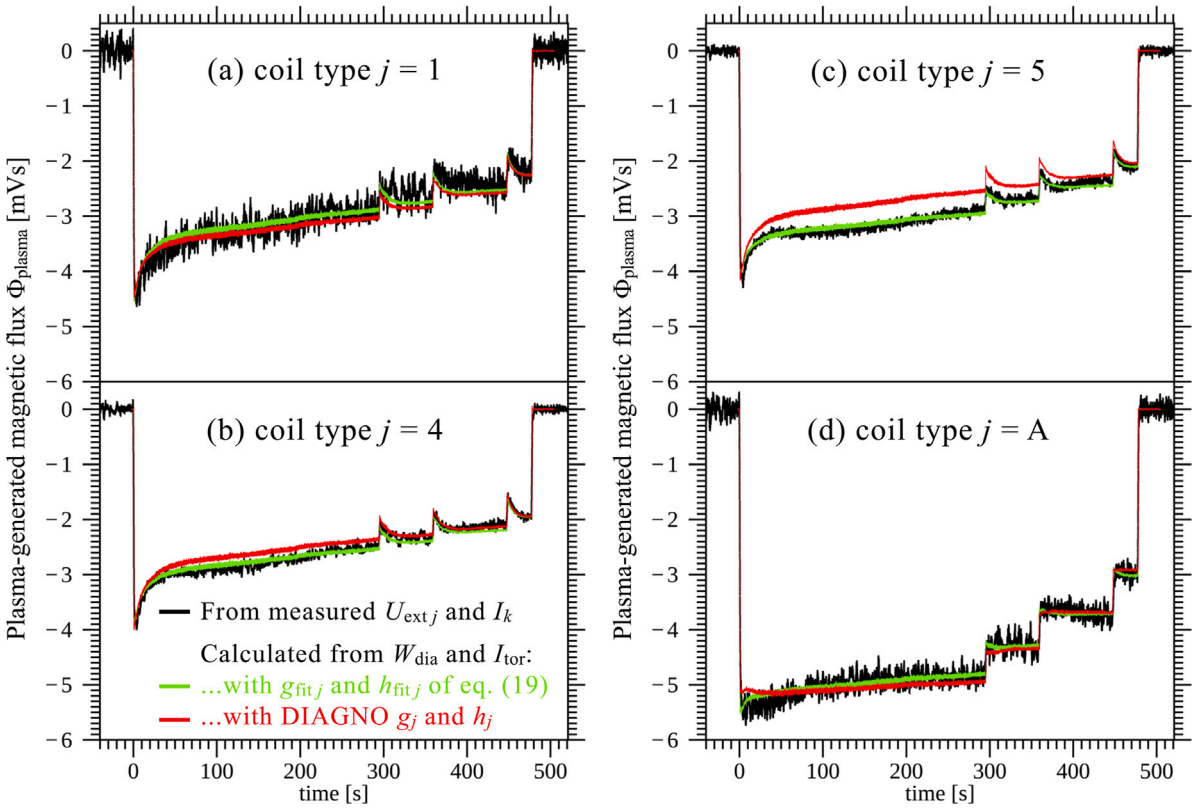

Fig. 25. Comparison of the single-loop magnetic fluxes $\Phi_{plasma\,j}$ from Eq. (2) (black), calculated from the measured $U_{ext\,j}$ and I_k signals of the coil circuits in discharge 20230215.032, with the linear combinations of W_{dia} and I_{tor} with the coefficients $g_{fit\,j}$ and $h_{fit\,j}$ of Eq. (19), and with the same linear combinations with the coefficients g_j and h_j from the DIAGNO simulations (see Section 4.1.2). The time traces for four of the seven coil circuits j are shown to provide examples for good and for not so good agreement.

In the present technical setup of the QD system, its internal voltages are not accessible and are only recorded if data storage is initiated, e. g., if the system is triggered. With our quantitative understanding we can now calculate the voltages in each QD unit from the diamagnetic energy and toroidal plasma current signals measured by the magnetic diagnostics (diamagnetic loop and Rogowski coil) — at least within the limits of precision to which the system parameters can be determined. This will be useful during operation, e. g., if we approach the trigger threshold of the QD system in a series of discharges. Actually, unusually fast decays of plasma energy and plasma current had also been observed in further W7-X discharges, without triggering the QD system. We analysed a few of these cases with our quantitative model and found that indeed in these cases the trigger thresholds had either not been exceeded, or had been exceeded not for a sufficiently long time interval, such that the integrating circuits in the QDUs smoothed out the voltage peaks.

With the detailed analysis and understanding of the system it was possible to suggest several ways to mitigate the problem in Section 5, without discussing in detail in this article the technical effort required to realise the different suggestions.

7.2. Field coils as magnetic diagnostics

As changes of the plasma-generated magnetic flux are reflected in the voltage and current signals of the field coils, we investigated, how well the diamagnetic energy and the toroidal plasma current can be derived from the field coil signals only. Such an approach was previously suggested and even realised in tokamaks [46,47] and in the LHD heliotron [48]. In LHD, measurements of the currents in the helical coil and in the various supporting steel structures were also used to correct the diamagnetic loop signal, since no compensation coils are available in that device. For W7-X the idea to use the superconducting coils as magnetic diagnostics appears particularly attractive, since the field coils promise to be mechanically and thermally more stable in long discharges than the pick-up coils of the magnetic diagnostics mounted inside the plasma vessel. In addition, in contrast to the helical windings at LHD, the W7-X field coils couple only weakly to the toroidal plasma current density, such that a good approximation of the plasma energy can be obtained without considering the toroidal plasma current. While such measurements cannot compete with the time resolution of in-vessel diagnostics, due to the shielding by plasma vessel and coil casings, the aim would be to use the measurement of field coil voltages and currents to complement the signals of the in-vessel magnetic diagnostics for long time intervals. For a later fusion reactor, it may be an attractive option to rely entirely on W_{dia} measurements with the field coils and to abandon a particular diamagnetic loop.

We explained in Section 6.2 that in the W7-X setup there are two options to use the field coil signals. For both options, the currents in the seven coil circuits are needed. In addition, for option 1, the voltages applied by the power supplies to these seven coil circuits must be measured and integrated. This is the option which could be used in any tokamak or stellarator, as only measurements at the coil power supplies are required. For option 2, instead, one or several voltages across the DLs of the field coils are needed, which again must be integrated. This requires that there exist connections to different points of the coil winding pack and it also requires that these connection points subdivide the winding asymmetrical either with respect to the plasma-generated magnetic flux or with respect to the inductance of the different sections of winding. It is therefore precisely that property of the W7-X QD system causing its sensitivity to changes of the plasma energy which can be utilised here.

Our analysis demonstrates that we can achieve good agreement between the diamagnetic energies derived from the field coil signals and the CWdia signal with both methods. We noted that the current signals of the coil circuits exhibit quite different noise levels. We should

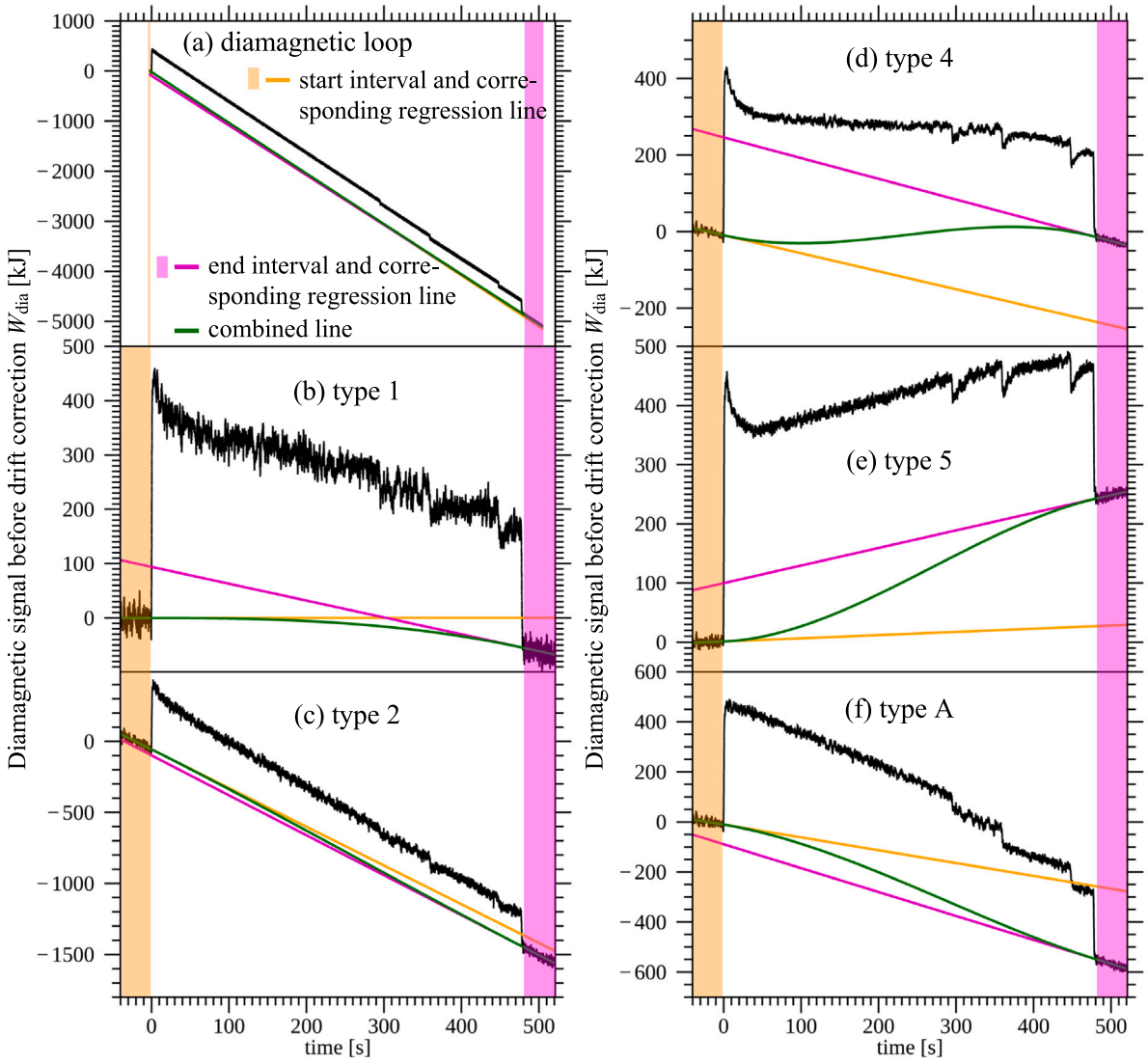

Fig. 26. W_{dia} calculated from the compensated signal of the diamagnetic loop (a) and from 5 of the 7 field coil circuit signals (b–f) for discharge 20230215.032 before removing offsets and offset drifts. Regression lines were calculated from an interval before plasma start (orange) and from an interval after the end of the plasma discharge (magenta). A combined line (green) was then calculated as cubic spline, which has the same value and slope as the orange line at the end of the orange time interval and the same value and slope as the magenta line at the beginning of the magenta time interval. This combined line was then subtracted from the signal to obtain the drift corrected curves shown in the previous sections (Figs. 22–25). The deviations of the magenta regression lines from the orange regression lines at the beginning of the magenta time interval and the differences in slope between the magenta and orange regression lines are listed in Table 7 for the diamagnetic loop signal and for the signals from all 7 field coil circuits.

keep in mind that we need to know the currents with a precision of few Ampères on a level of order 10 kA. On the one hand side those coil circuits with low noise level indicate that there is potential for improvement in the other circuits. On the other hand side, the noise level is not really a problem if we are considering time scales of several seconds, since the noise can then be reduced by averaging over several thousand samples. This is visible in the analysis of the very long discharge 20230215.032 in Section 6.4.1.

For the integration of the voltage signals over long time intervals, offset drifts are a notorious problem. The drifts can have various origins, like thermovoltages in the cables between sensors and analog-to-digital converters, thermal drifts in intermediate amplifiers etc., as has been discussed in detail in [25,26] for the case of the W7-X magnetic equilibrium diagnostics. The solution to minimise the effect of such drifts for the W7-X magnetic measurements was the design of a specialised data acquisition system [26,45], which was, however, not in use for the voltage signals from the field coil circuits. Such offset drifts are indicated by differences in the regression lines taken without plasma in intervals just before the beginning of the plasma discharge and just after the end of the plasma discharge. As demonstrated in Section 6.4.3, the differences in the regression lines are indeed mostly larger for the signals derived from the field coil circuits than for the CWdia signal with its specialised data acquisition system.

The QD voltages (option 2 for measuring the flux changes induced in the field coils) have so far not been regularly available and are presently recorded only for intervals of 10 s. In order to make use of them, the voltage across one or several double layers should be measured independently of the QDUs, preferably across DLs 1+2 of one of the non-planar coils.

As a next step, one could record the voltage applied to one of the field coil circuits $U_{ext\,j}$ with the specialised electronics under use for the equilibrium magnetic diagnostics in order to find out whether the offset drift can thus be reduced.

8. Conclusions

The induced voltages in the W7-X superconducting field coils due to changes in the plasma-generated magnetic flux and the ensuing

Table 7
Deviations ΔW_{dia} between a regression line calculated from an interval before plasma start (orange lines in Fig. 26) and a regression line calculated from an interval after the end of the plasma discharge (magenta lines in Fig. 26) at the end of the plasma discharge and difference in slopes $\Delta b_{regress}$ between the orange and magenta lines for the compensated diamagnetic loop signal and the W_{dia} signals calculated from the 7 field coil circuits for discharge 20230215.032.

	Diamagnetic loop	Field coil type j						
		1	2	3	4	5	A (= 6)	B (= 7)
ΔW_{dia} [kJ]	+37	−56	−84	+105	+222	+216	−292	+445
$\Delta b_{regress}$ [kJ/s]	+0.23	−0.31	−0.09	−0.41	−0.07	+0.24	−0.44	+0.07

changes in coil currents were modelled. The results agree well with the measured voltages in the QD system during changes in plasma energy and toroidal plasma current. The main contribution to these voltages is due to the difference in induced voltage between the radially stacked double layers of the coil windings during changes of the coil currents.

During intervals with high rates of change of the plasma energy, the QD voltages can be large enough to trigger a fast ramp-down of the coil currents, as it was observed in two W7-X discharges, due to sudden influx of impurities into the plasma. The same could indeed occur at sufficiently high heating power and good energy confinement at a sudden shutdown of the full heating power.

This behaviour is a result of the particular winding scheme of the W7-X coils in conjunction with the particular setup of the QD system. Several different modifications of the QD system were described which could mitigate the problem. For the next operational phase of W7-X, the settings of the QD system have been adapted, and the present simplified redundancy QD system ("backup system"), which is particularly sensitive to changes of plasma-generated magnetic flux, will be replaced by a full second version of the primary system as a next step. The modelling capability described in this paper will be used to calculate the expected QD voltages from the signals of the diamagnetic loop and the Rogowski coil and to assess the margin before triggering the QD system, even if the QD voltages are not recorded.

We demonstrated that the diamagnetic energy can be derived entirely from the currents and voltages in the superconducting coil circuits, in good agreement with the measurements of the diamagnetic loop with compensation coils. This is possible in two different ways, both using the coil currents in the 7 different superconducting coil circuits, plus either with the voltage of one of the coil power supplies, or with one of the voltages across a DL. In both cases, the voltage signals need to be integrated, which represents the usual challenge of offset drifts in long-pulse discharges. Whereas only the existing electronics and data acquisition systems of the coil circuits have been used to demonstrate this application, the long-term drift challenge may be mitigated by applying the specialised data acquisition systems developed for the W7-X equilibrium magnetics. A test with such a system would be the next step in the use of field coils for diamagnetic energy measurements on W7-X.

CRediT authorship contribution statement

M. Endler: Writing – review & editing, Writing – original draft, Visualization, Validation, Supervision, Software, Methodology, Investigation, Formal analysis, Data curation, Conceptualization. **K. Rieße:** Writing – review & editing, Software, Resources, Methodology, Investigation, Formal analysis, Data curation, Conceptualization. **J. Geiger:** Writing – review & editing, Software, Resources, Methodology, Investigation, Formal analysis, Data curation. **K. Rahbarnia:** Writing – review & editing, Software, Resources, Methodology, Investigation, Formal analysis, Data curation. **M. Schneider:** Software, Resources, Data curation. **V. Bykov:** Writing – review & editing, Data curation. **M. Khokhlov:** Visualization, Software, Resources, Methodology, Formal analysis, Data curation. **D. Zhang:** Visualization, Software, Resources, Formal analysis, Data curation.

Declaration of competing interest

The authors declare the following financial interests/personal relationships which may be considered as potential competing interests: All authors report financial support and article publishing charges were provided by European Consortium for the Development of Fusion Energy. They declare that they have no further known competing financial interests or personal relationships that could have appeared to influence the work reported in this paper.

Acknowledgements

We wish to thank B. Buttenschön, Y. Gao, C. Killer, A. Knieps, E. Köster, S. A. Lazerson, Th. Mönnich, Th. Rummel, F. Wagner and M. Zanini for important information and useful suggestions and discussions, Th. Sieber and M. Banduch for providing updated coil models for the computation of double layer inductances, and M. Otte and R. C. Wolf for their support and encouragement.

This work has been carried out within the framework of the EUROfusion Consortium, funded by the European Union via the Euratom Research and Training Programme (Grant Agreement No 101052200 — EUROfusion). Views and opinions expressed are however those of the authors only and do not necessarily reflect those of the European Union or the European Commission. Neither the European Union nor the European Commission can be held responsible for them.

Data availability

Data will be made available on request.

References

[1] T. Sunn Pedersen, et al., the W7-X Team, Experimental confirmation of efficient island divertor operation and successful neoclassical transport optimization in Wendelstein 7-X, Nucl. Fusion 62 (4) (2022) 042022, http://dx.doi.org/10.1088/1741-4326/ac2cf5.

[2] G. Grieger, C. Beidler, E. Harmeyer, W. Lotz, J. Kißlinger, P. Merkel, J. Nührenberg, F. Rau, E. Strumberger, H. Wobig, Modular stellarator reactors and plans for Wendelstein 7-X, Fusion Technol. 21 (3P2B) (1992) 1767–1778, http://dx.doi.org/10.13182/FST92-A29977.

[3] H.-S. Bosch, et al., Technical challenges in the construction of the steady-state stellarator Wendelstein 7-X, Nucl. Fusion 53 (12) (2013) 126001, http://dx.doi.org/10.1088/0029-5515/53/12/126001.

[4] J. Sapper, W. Gardebrecht, F. Kerl, I. Schoenwolf, The layout of the Wendelstein 7-X magnet, Fusion Eng. Des. 58–59 (2001) 237–240, proceedings of the 21st Symposium on Fusion Technology, Madrid, Spain, 11–15 2000.

[5] L. Wegener, J.-H. Feist, J. Sapper, F. Kerl, F. Werner, Final design and construction of the Wendelstein 7-X coils, Fusion Eng. Des. 58–59 (2001) 225–230, Proceedings of the 21st Symposium on Fusion Technology, Madrid, Spain, 11–15 2000.

[6] T. Rummel, K. Rieße, G. Ehrke, K. Rummel, A. John, T. Mönnich, K.-P. Buscher, W.H. Fietz, R. Heller, O. Neubauer, A. Panin, The superconducting magnet system of the stellarator Wendelstein 7-X, IEEE Trans. Plasma Sci. 40 (3) (2012) 769–776, special Issue on 24th Symposium on Fusion Engineering (SOFE 2011), June 25–June 30 2011, Chicago, IL.

[7] R.K. Maix, V. Bagnato, M. Fricke, K. Heyn, T. Kluck, F. Lange, K. Rieße, C. Sborchia, N. Valle, Design, production and QA test results of the NbTi CIC conductors for the W7-X magnet system, J. Phys. Conf. Ser. 43 (2006) 753–758, Proceedings of 7th European Conference on Applied Superconductivity, 11–15 September 2005, Vienna, Austria.

[8] K. Sedlak, P. Bruzzone, T. Rummel, M. Nagel, Study of the hot-spot temperature during quench in the nonplanar coils of W7-X, IEEE Trans. Appl. Supercond. 28 (3) (2018) 4200905, Proceedings of the 25th International Conference on Magnet Technology, RAI Congress Center, Amsterdam, The Netherlands, August 27–September 1 2017.

[9] K. Risse, T. Rummel, H.-S. Bosch, V. Bykov, A. Carls, F. Füllenbach, T. Mönnich, M. Nagel, M. Schneider, W7-X Team, The magnet system of Wendelstein 7-X stellarator in operation, Fusion Eng. Des. 136 (part A) (2018) 12–16, http://dx.doi.org/10.1016/j.fusengdes.2015.02.067, Proceedings of the 13th International Symposium On Fusion Nuclear Technology (ISFNT-13), Kyoto, Japan, 2017.

[10] J.L. Duchateau, J.Y. Journeaux, B. Gravil, Tore Supra superconducting toroidal magnetic field system, Fusion Sci. Technol. 56 (3) (2009) 1092–1123, http://dx.doi.org/10.13182/FST09-A9170, Special Issue on Tore Supra.

[11] Y. Chu, H. Yonekawa, Y.O. Kim, K.R. Park, H.J. Lee, M.K. Park, Y.M. Park, S.J. Lee, T.H. Ha, Y.K. Oh, J.S. Bak, KSTAR Team, Quench detection based on voltage measurement for the KSTAR superconducting coils, IEEE Trans. Appl. Supercond. 19 (3) (2009) 1565–1568, Proceedings of the 2008 Applied Superconductivity Conference, Chicago, IL, August 17–22, 2008, Part II.

[12] P.D. Weng, Z.M. Chen, Y. Wu, Y.F. Tan, Quench current measurement and performance evaluation of the EAST toroidal field coils, Fusion Eng. Des. 75–79 (2005) 143–148, Proceedings of the 23rd Symposium on Fusion Technology (SOFT 23), Venice, Italy, 20–24 Sept. 2004.

[13] M. Coatanea, J.-L. Duchateau, S. Nicollet, B. Lacroix, F. Topin, Investigations about quench detection in the ITER TF coil system, IEEE Trans. Appl. Supercond. 22 (3) (2012) 4702404, http://dx.doi.org/10.1109/TASC.2011.2178979, Proceedings of the 22nd International Conference on Magnet Technology (MT-22), Marseille, France, September 12–16, 2011.

[14] A.N. Sharma, C.J. Hansalia, Y. Yeole, G. Bansal, S. Pradham, A. Motira, Y.C. Saxena, Quench detection and data acquisition system for SST-1 superconducting magnets, Fusion Eng. Des. 74 (2005) 819–823, Proceedings of the 23rd Symposium on Fusion Technology (SOFT 23), Venice, Italy, 20–24 Sept. 2004.

[15] R.C. Wolf, et al., Major results from the first plasma campaign of the Wendelstein 7-X stellarator, Nucl. Fusion 57 (10) (2017) 102020, http://dx.doi.org/10.1088/1741-4326/aa770d.

[16] T. Sunn Pedersen, A. Dinklage, Y. Turkin, R. Wolf, S. Bozhenkov, J. Geiger, G. Fuchert, H.-S. Bosch, K. Rahbarnia, H. Thomsen, U. Neuner, T. Klinger, A. Langenberg, H.T. Mora, P. Kornejew, J. Knauer, M. Hirsch, W7-X Team, N. Pablant, Key results from the first plasma operation phase and outlook for future performance in Wendelstein 7-X, Phys. Plasmas 24 (5) (2017) 055503, http://dx.doi.org/10.1063/1.4983629.

[17] T. Klinger, A. Alonso, S. Bozhenkov, R. Burhenn, A. Dinklage, G. Fuchert, J. Geiger, O. Grulke, A. Langenberg, M. Hirsch, G. Kocsis, J. Knauer, A. Krämer-Flecken, H. Laqua, S. Lazerson, M. Landreman, H. Maaßberg, S. Marsen, M. Otte, N. Pablant, E. Pasch, K. Rahbarnia, T. Stange, T. Szepesi, H. Thomsen, P. Traverso, J.L. Velasco, T. Wauters, G. Weir, T. Windisch, The Wendelstein 7-X Team, Performance and properties of the first plasmas of Wendelstein 7-X, Plasma Phys. Control. Fusion 59 (1) (2017) 014018, http://dx.doi.org/10.1088/0741-3335/59/1/014018, Special Issue featuring the invited talks from the 43rd EPS Conference on Plasma Physics, Leuven, 4–8 Jul. 2016.

[18] K. Rieße, T. Rummel, G. Ehrke, M. Köppen, Design, tests, and repair procedures for the electrical insulation of the superconducting W7-X magnets, IEEE Trans. Appl. Supercond. 20 (3) (2010) 447–450, http://dx.doi.org/10.1109/TASC.2010.2044030, Proceedings of the 21st International Conference on Magnet Technology, Hefei, Anhui, China, August 27–31, 2009.

[19] S. Kim, K. Chung, D.K. Lee, A continuous winding scheme for superconducting tokamak coils with cable-in-conduit conductor, Fusion Eng. Des. 55 (1) (2001) 21–33.

[20] V. Tomarchio, P. Barabaschi, A. Cucchiaro, P. Decool, A. Della Corte, A. Di Zenobio, D. Duglue, L. Meunier, L. Muzzi, M. Nannini, M. Peyrot, G. Philips, A. Pizzuto, C. Portafaix, L. Reccia, K. Yoshida, L. Zani, Design of the JT-60SA superconducting toroidal field magnet, IEEE Trans. Appl. Supercond. 20 (3) (2010) 572–575, http://dx.doi.org/10.1109/TASC.2010.2041335, Proceedings of the 21st International Conference on Magnet Technology, Hefei, Anhui, China, August 27–31, 2009.

[21] D. Birus, T. Rummel, M. Fricke, K. Petry, H. Demattio, Development of quench detection system for W7-X, Fusion Eng. Des. 82 (5–14) (2007) 1400–1405, Proceedings of the 24th Symposium on Fusion Technology (SOFT-24), Warsaw, Poland, 11–15 September 2006.

[22] D. Birus, M. Schneider, T. Rummel, M. Fricke, K. Petry, A. Ebersoldt, Processing of the quench detection signals in W7-X, Fusion Eng. Des. 84 (7–11) (2009) 457–460, Proceedings of the 25th Symposium on Fusion Technology (SOFT-25), Rostock, Germany, 15–19 September 2008.

[23] D. Birus, M. Schneider, T. Rummel, M. Fricke, The quench detection system of Wendelstein 7-X, Fusion Eng. Des. 86 (6–8) (2011) 1566–1570, Proceedings of the 26th Symposium on Fusion Technology (SOFT-26), Porto, Portugal, September 27–October 1 2010.

[24] K. Risse, M. Lewandowska, A. Dembkowska, T. Rummel, H.-S. Bosch, W7-X Team, Thermo-hydraulic calculations on W7-X coils for updated quench detection parameters, IEEE Trans. Appl. Supercond. 34 (5) (2024) 4206605, http://dx.doi.org/10.1109/TASC.2024.3376634, Proceedings of the 28th International Conference on Magnet Technology, Aix-en-Provence, France, 10–15 September 2023, Part 1.

[25] M. Endler, B. Brucker, V. Bykov, A. Cardella, A. Carls, F. Dobmeier, A. Dudek, J. Fellinger, J. Geiger, K. Grosser, O. Grulke, D. Hartmann, D. Hathiramani, K. Höchel, M. Köppen, R. Laube, U. Neuner, X. Peng, K. Rahbarnia, K. Rummel, T. Sieber, S. Thiel, A. Vorköper, A. Werner, T. Windisch, M.Y. Ye, Engineering design for the magnetic diagnostics of Wendelstein 7-X, Fusion Eng. Des. 100 (2015) 468–494, http://dx.doi.org/10.1016/j.fusengdes.2015.07.020.

[26] K. Rahbarnia, H. Thomsen, U. Neuner, J. Schilling, J. Geiger, G. Fuchert, T. Andreeva, M. Endler, D. Hathiramani, T. Bluhm, M. Zilker, B.B. Carvalho, A. Werner, Wendelstein 7-X Team, Diamagnetic energy measurement during the first operational phase at the Wendelstein 7-X stellarator, Nucl. Fusion 58 (9) (2018) 096010, http://dx.doi.org/10.1088/1741-4326/aacab0.

[27] D. Zhang, R. Burhenn, C.D. Beidler, Y. Feng, H. Thomsen, C. Brandt, S. Buller, F. Reimold, P. Hacker, R. Laube, J. Geiger, J.M. García Regaña, H.M. Smith, R. König, L. Giannone, F. Penzel, T. Klinger, J. Baldzuhn, S. Bozhenkov, T. Bräuer, J.K. Brunner, B. Buttenschön, H. Damm, M. Endler, F. Effenberg, G. Fuchert, Y. Gao, M. Jakubowski, J. Knauer, T. Kremeyer, M. Krychowiak, S. Kwak, H.P. Laqua, A. Langenberg, M. Otte, N. Pablant, E. Pasch, K. Rahbarnia, A. Pavone, L. Rudischhauser, J. Svensson, C. Killer, T. Windisch, W7-X Team, Bolometer tomography on Wendelstein 7-X for study of radiation asymmetry, Nucl. Fusion 61 (11) (2021) 116043.

[28] M. Zanini, B. Buttenschön, H.P. Laqua, H. Thomsen, T. Stange, C. Brandt, H. Braune, K.J. Brunner, A. Dinklage, Y. Gao, M. Hirsch, U. Höfel, J. Knauer, S. Marsen, N. Marushchenko, A. Pavone, K. Rahbarnia, J. Schilling, Y. Turkin, R.C. Wolf, A. Zocco, W7-X Team, Confinement degradation and plasma loss induced by strong sawtooth crashes at W7-X, Nucl. Fusion 61 (11) (2021) 116053, http://dx.doi.org/10.1088/1741-4326/ac2870.

[29] K. Aleynikova, S.R. Hudson, P. Helander, A. Kumar, J. Geiger, M. Hirsch, J. Loizu, C. Nührenberg, K. Rahbarnia, Z. Qu, Y. Gao, H. Thomsen, Y. Turkin, M. Zanini, W7-X Team, Model for current drive induced crash cycles in W7-X, Nucl. Fusion 61 (12) (2021) 126040, http://dx.doi.org/10.1088/1741-4326/ac2ab9.

[30] D. Nicolai, V. Borsuk, P. Drews, O. Grulke, K.P. Hollfeld, T. Krings, Y. Liang, C. Linsmeier, O. Neubauer, G. Satheeswaran, B. Schweer, G. Offermans, W7-X Team, A multi-purpose manipulator system for W7-X as user facility for plasma edge investigation, Fusion Eng. Des. 123 (2017) 960–964, Proceedings of the 29th Symposium on Fusion Technology (SOFT-29), Prague, Czech Republic, September 5–9, 2016.

[31] C. Killer, Y. Gao, V. Perseo, L. Rudischhauser, K. Hammond, B. Buttenschön, T. Barbui, B.D. Blackwell, K.-J. Brunner, P. Drews, M. Endler, J. Geiger, O. Grulke, M. Jakubowski, S. Klose, J. Knauer, A. Knieps, R. König, Y. Li, U. Neuner, H. Niemann, M. Otte, J. Schilling, A. Puig Sitjes, K. Rahbarnia, T. Stange, W7-X Team, Effect of toroidal plasma currents on the Wendelstein 7-X scrape-off layer, Plasma Phys. Control. Fusion 61 (12) (2019) 125014, http://dx.doi.org/10.1088/1361-6587/ab4f2d.

[32] W. Biel, A. Greiche, R. Burhenn, E. Jourdain, D. Lepere, High efficiency extreme ultraviolet overview spectrometer: Construction and laboratory testing, Rev. Sci. Instrum. 77 (10) (2006) 10F305, Proceedings of the 16th Topical Conference on High-Temperature Plasma Diagnostics, Williamsburg, VA, USA, 7–11 May 2006.

[33] W.A. Cooper, A.J. Wootton, β_p analysis for tokamak plasma with anisotropic pressure and mass flow, Plasma Phys. 24 (9) (1982) 1183–1185.

[34] T. Yamaguchi, K.Y. Watanabe, S. Sakakibara, Y. Narushima, K. Narihara, T. Tokuzawa, K. Tanaka, I. Yamada, M. Osakabe, H. Yamada, K. Kawahata, K. Yamazaki, LHD Experimental Group, Measurement of anisotropic pressure using magnetic measurements in LHD, Nucl. Fusion 45 (11) (2005) L33–L36.

[35] S. Besshou, C.E. Thomas, T. Ohba, A. Iiyoshi, K. Uo, Diamagnetism and beta in beam heated currentless plasmas of Heliotron E, Nucl. Fusion 26 (10) (1986) 1339–1348.

[36] V.D. Pustovitov, Refined theory of diamagnetic effect in stellarators, J. Plasma Fusion Res. 69 (1) (1993) 34–40.

[37] H.J. Gardner, Modelling the behaviour of the magnetic field diagnostic coils on the W VII-AS stellarator using a three-dimensional equilibrium code, Nucl. Fusion 30 (8) (1990) 1417–1424.

[38] J. Geiger, C.D. Beidler, Y. Feng, H. Maaßberg, N.B. Marushchenko, Y. Turkin, Physics in the magnetic configuration space of W7-X, Plasma Phys. Control. Fusion 57 (1) (2015) 014004, http://dx.doi.org/10.1088/0741-3335/57/1/014004.

[39] G. Grieger, W. Lotz, P. Merkel, J. Nührenberg, J. Sapper, E. Strumberger, H. Wobig, W7-X Team, R. Burhenn, V. Erckmann, U. Gasparino, L. Giannone, H.J. Hartfuß, R. Jaenicke, G. Kühner, H. Ringler, A. Weller, F. Wagner, W7-AS Team, Physics optimization of stellarators, Phys. Fluids B: Plasma Phys. 4 (7) (1992) 2081–2091.

[40] J. Geiger, M. Endler, A. Werner, Magnetic diagnostics for equilibrium reconstruction at W7-X, Contrib. Plasma Phys. 50 (8) (2010) 736–740, Special Issue: Proceedings of 17th International Stellarator/Heliotron Workshop, October 12–16, 2009, Princeton Plasma Physics Laboratory (PPPL), Princeton, New Jersey, USA (Part II).

[41] F. Schauer, E. Harmeyer, B. Hein, Wirbelstromkräfte auf das W7-X-Plasmagefäß durch Plasmastromabbrüche, Tech. Rep., Max–Planck-Institut für Plasmaphysik, Greifswald, 2009.

[42] ABB Industrie AG, Technische Spezifikation Bus und Kabelverbindungen, Istzustand, Tech. Rep., Max–Planck-Institut für Plasmaphysik, Greifswald, 2013.
[43] Home page of ANSYS Maxwell (Low Frequency Electromagnetic Field Simulation), https://www.ansys.com/en-gb/products/electronics/ansys-maxwell.
[44] Y. Hu, J. Li, B. Shen, H. Lv, Y.Z. Xiao, Study of electromagnetic noise influence on quench detection system under different discharge conditions for EAST, Fusion Eng. Des. 88 (2) (2013) 73–78.
[45] A. Werner, W7-X magnetic diagnostics: Performance of the digital integrator, Rev. Sci. Instrum. 77 (10) (2006) 10E307, Proceedings of the 16th Topical Conference on High-Temperature Plasma Diagnostics, Williamsburg, VA, USA, 7–11 May 2006.
[46] P. Thomas, Diamagnetic Flux Measurement using the PDX TF Coils, Tech. Rep. PPPL-1979, Princeton Plasma Physics Laboratory, Princeton, 1983.
[47] J. Yang, Y. Kim, W.I. Jeong, Y.S. Hwang, Simple and accurate method of diamagnetic flux measurement in Versatile Experimental Spherical Torus (VEST), Rev. Sci. Instrum. 89 (10) (2018) 103508.
[48] K. Hamamura, K. Yamazaki, H. Chikaraishi, S. Sakakibara, N. Yanagi, T. Shoji, T. Watari, A new method for measuring plasma energy using superconducting helical coils, Fusion Eng. Des. 81 (23–24) (2006) 2827–2830, http://dx.doi.org/10.1016/j.fusengdes.2006.07.035, Proceedings of the 15th Toki Conference on Fusion and Advanced Technology, 6–9 December 2005, Toki-city, Japan.
[49] S. Sakakibara, H. Yamada, LHD Experiment Group, Magnetic measurements in LHD, Fusion Sci. Technol. 58 (1) (2010) 471–481, http://dx.doi.org/10.13182/FST10-A10833, Special Issue on Large Helical Device (LHD).